Non-local dynamic behavior of linear fiber reinforced materials

Jean Soubestre, Claude Boutin

Non-local dynamic behavior of linear fiber reinforced materials

Jean Soubestre [a,*], Claude Boutin [b]

[a] CETE Ile-de-France, MEDDE, rue de l'Egalité Prolongée BP 134, 93352 Le Bourget Cedex, France
[b] Université de Lyon, Ecole Nationale des Travaux Publics de l'Etat (ENTPE), DGCB, CNRS 3237, 3 rue Maurice Audin, 69518 Vaulx-en-Velin Cedex, France

ABSTRACT

This article deals with the effective dynamic behavior of elastic materials periodically reinforced by stiff linear slender elastic inclusions. By assuming a small scale ratio ε between the period section size and the characteristic size of the system global strain, and by weighing the constituents stiffness contrast by powers of ε, the dynamic macroscopic behavior at the leading order is derived through the asymptotic homogenization method of periodic media considering different frequency ranges. A two order stiffness contrast ($\mu_m/\mu_p \quad O(\varepsilon^2)$) is shown to lead to a dynamic macroscopic behavior spatially non-local in the transverse direction, where the system behaves as a generalized inner bending continuum, and temporally non-local in the axial direction, where the system behaves, at higher frequency, as a metamaterial in which internal resonance phenomena take place. The consequences of such non-localities on the reinforced medium modes are examined. The system axial and transverse modes are shown to be significantly different from those of usual composites.

1. Introduction

This paper is concerned with the dynamic response of materials reinforced by stiff linear fibers. These highly contrasted media consist in a matrix in which long and stiff inclusions, orientated along a single direction, are embedded. Such materials are nowadays in frequent use in different engineering domains, either as hand-made industrial materials, for instance in aeronautics (mat of carbon or glass fibers, ...), in civil engineering (reinforced concrete, rigid inclusions fields, deep foundations,...), or as natural elements investigated in biomechanics (bones, vegetal tissues,...).

Practical applications generally involve a large number of fibers and the individual description of each constituent is often impossible and generally not necessary. Indeed, heterogeneous media can be described as equivalent continuous media, provided that (i) the media morphology is sufficiently regular to be described by a representative volume element (RVE) and that (ii) a scale separation condition is fulfilled between the characteristic size L of the studied phenomena, that should be significantly larger than the RVE size, and l (Auriault, 1991), i.e. $\varepsilon = l/L \ll 1$. These physical conditions are explicitly used in a rigorous mathematical way in the asymptotic homogenization method of periodic media (Bensoussan et al., 1978; Sanchez-Palencia, 1980), where the period Ω plays the role of the RVE. This method presents the great advantage of building up the macroscopic behavior (governing differential system and effective properties) from the RVE morphology (geometry), the properties of the constituents and the local balances, without any other requirement than scale separation.

A straight application of this method to usual composites leads to an equivalent Cauchy medium whose effective elastic tensor is determined by the material microstructure (Léné, 1978; Sanchez-Palencia, 1980; Postel, 1985 for periodic fiber composites) and whose effective density is the mean density. In quasi-statics, when considering higher order description, correctors appear and the macroscopic description involves higher gradient of the macroscopic strain (Gambin and Kröner, 1989; Boutin, 1996). Thus,

* Corresponding author.
E-mail addresses: jean.soubestre@developpement-durable.gouv.fr (J. Soubestre), claude.boutin@entpe.fr (C. Boutin).

the medium behaves as a "slightly" generalized medium with "non-local" second gradient effect of small amplitude. In dynamics, higher order correctors also arise on the inertia that induces an additional "slight" non-local effect in time to be accounted for when describing wave scattering (cf. Boutin and Auriault, 1993). In this paper, "non-local" denomination is meant by reference to the classic description. For space non-locality, since the strain gradient(s) is involved, the knowledge of the strain state in the RVE (local in space) is not sufficient: the strain gradient requires the knowledge of the strain state in the neighboring RVE (spacial non-locality). Similarly, for time non-locality, the instantaneous acceleration (local in time) is not sufficient and the knowledge of acceleration at previous time is necessary (time non-locality).

Stiff fiber reinforced materials depart from usual composites in two non conventional key features. First, the mechanical properties of the constituents are highly contrasted. Second, the axial geometry of each fiber is continuous over a long distance, much larger than the RVE size (in direction perpendicular to the fiber). It leads to infer that the so-called non-local effects could arise *at the leading order* instead of arising as correctors. In fact, in addition to the usual shear response of the soft matrix, one may expect from the long fibers a bending effect, that corresponds to a second gradient non-local effect. Furthermore, for a particular frequency range corresponding to large wavelengths (compared to the RVE size) carried by the stiff fibers, the matrix may reach a dynamic regime at the local scale, giving an inner resonance effect that results in a non-local effect in time.

In quasi-statics, several studies argue in favor of non-local effects at the leading order for elastic media made of soft matrix and stiff fibers. By studying a single stiff beam in a soft matrix, Caillerie (1980) identified an enriched kinematics at the leading order. For periodically reinforced systems undergoing uniform distortion kinematics, Pideri and Seppecher (1997) and Bellieud and Bouchitté (1997) show through an asymptotic approach based on energy (see also Dell'Isola et al. (1995)), that both shear and bending effects remain in the macro energy. For the same kind of materials and kinematics, De Buhan and Sudret (1999) developed a "multiphase approach" that accounts for shear effects from the matrix and inner bending effects from the inclusions. Recently, through the homogenization method of periodic media, Boutin and Soubestre (2011) derived the macroscopic behavior of those media under general kinematics. They show that a two order stiffness contrast (i.e. $O(\varepsilon^2)$) leads to a generalized continuum. For transverse kinematics, inner bending from the reinforcements together with shear from the matrix are involved at the same order; while axial kinematics is governed by the reinforcements compression.

In dynamics of composites presenting a two order stiffness contrast with a stiff component connected, the inner resonance occurence has been evidenced in the pioneer paper by Auriault and Bonnet (1985). The effect is shown to drastically modify the dynamics of the system at frequencies close to eigen frequencies of the soft domain. Such inner resonating materials, now called "metamaterials", recently received further attention. Experiments on contrasted composites made of epoxy matrix-duraliminium cylinders (Vasseur et al., 1998) or made of epoxy matrix embedding lead spheres coated by silicon rubber (Liu et al., 2000) clearly demonstrate the existence of band gaps related to local resonances. The theoretical mathematical study of the inner resonance has been investigated by Zhikov (2000) and Avila et al. (2005) (for fiber composites). Babych et al. (2008) and Smyshlyaev (2009), follow the same line and provide results on the convergence of the asymptotic approach. For reticulated structures experiencing global vibrations, inner resonance related to bending has also been evidenced in Boutin et al. (2010).

The aim of this paper is to explore these phenomena and to identify the consequences on the modal features of a layer made of such a material. The study focuses on an elastic matrix (indice m) periodically reinforced by linear stiff elastic inclusions (indice p) oriented in the same direction, presenting a two-order stiffness contrast ($\mu_m/\mu_p = O(\varepsilon^2)$). It is shown that both space and time non-local effects can appear according to the kinematics and the frequency range. More precisely, the reinforced medium is spatially non-local in the transverse direction, where the system behaves as a generalized inner bending continuum, and temporally non-local in the axial direction, where the system behaves as a metamaterial. The high stiffness contrast associated with the oriented fiber geometry implies a high anisotropy. Hence, the frequency range associated with the dynamics in presence of inner bending (e.g. transverse mode) is one order smaller than the dynamics in presence of inner resonance (axial compression mode).

The paper is divided into five Sections. Section 2 presents the asymptotic method in the context of the dynamics of highly contrasted fiber reinforced media. The derivation of the quasi-static homogenized modelling is summarized in Section 3, following the approach developed in Boutin and Soubestre (2011). The homogenized model in dynamic regime is established in Section 4, evidencing different frequency ranges and phenomena: second gradient (namely bending) effects for the transverse kinematics, inner resonance effects for the axial dynamics. The modal analysis of a reinforced layer is conducted in Section 5 considering several *ad hoc* boundary conditions for such a medium and investigating successively transverse and axial modes.

2. Asymptotic approach of fiber reinforced medium

2.1. Studied composite and two-scale variables

The studied composite, of infinite lateral extension, is constituted by a matrix (index m) in which a periodic lattice of parallel identical homogeneous straight beams (index p) is embedded with a perfect contact (Fig. 1 (a)). Both constituents have an isotropic linear elastic behavior. They are characterized by their Lame coefficients λ_q and μ_q ($q = m, p$) or, equivalently, by their Young's modulus E_q and Poisson's ratio ν_q. Their density are denoted by ρ_q. Such media present a 2D-period $S : S = S_p \cup S_m$, where S_p stands for the beam section and S_m for the matrix section.

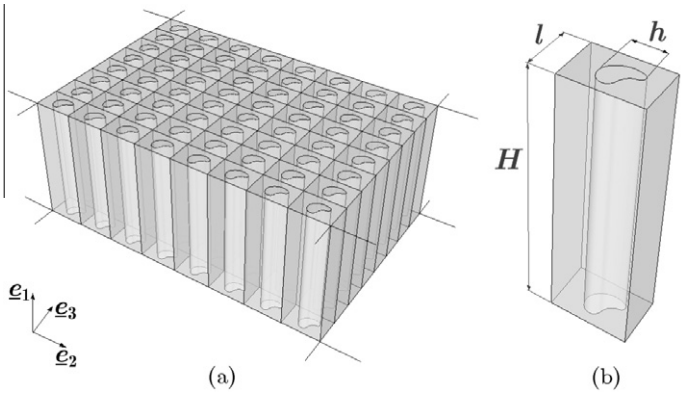

Fig. 1. Fiber reinforced material. (a) Periodic lattice of parallel identical homogeneous straight beams embedded in a matrix. (b) Period geometry and dimensions.

The interface between the two constituents is denoted $\Gamma = \partial S_p \cap \partial S_m$ and the period contour ∂S (Fig. 2). The concentration of reinforcement c is defined as the surface ratio $c = |S_p|/|S|$.

The dimension H along the beam axis is significantly larger than the lateral dimension l of the period (Fig. 1 (b)). The typical size of the beam section h is of the same order than l (Fig. 1 (b)), so that reinforcements may be in finite concentration. By considering phenomena involving a macroscopic length L much larger than l (and less or equal to H, i.e. $l \ll L \leqslant H$), the scale parameter of the problem, as used in the asymptotic expansions, is defined by:

$$\varepsilon = l/L \ll 1$$

The geometry naturally introduces a distinction between the axial direction (unit vector $\underline{a}_1$) and the directions in the plane of the section (unit vectors $\underline{a}_\alpha$ with $\alpha = 2, 3$). Herein, Greek indices run from 2 to 3 and Latin ones from 1 to 3. The relevant dimensionless space variables are $(x_i/L, x_\alpha/l)$ and the appropriate physical space variables are (x_i, y_α), where $y_\alpha = (L/l)x_\alpha = \varepsilon^{-1}x_\alpha$. Thus, any function $f(x_i)$ is rewritten as $f(x_i, y_\alpha)$ and its gradient becomes $\partial f/\partial x_i \underline{a}_i + \varepsilon^{-1}\partial f/\partial y_\alpha \underline{a}_\alpha$. According to the scale separation assumption and to the in-plane periodic geometry of the studied composite, variables related to the matrix are S-periodic. For example, the displacements in both constituents (ante-exponent $q = m, p$) are looked for in the form

$$^q\underline{u} = {}^q u_j(x_i, y_\alpha)\underline{a}_j \quad \text{with} \quad {}^m\underline{u}\ S-\text{periodic in } y_\alpha.$$

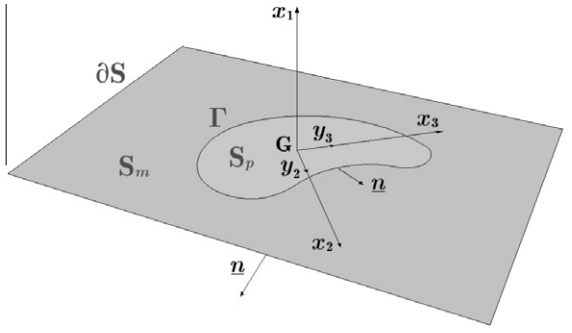

Fig. 2. Notations of the fiber reinforced material period section.

Notice also that:

$$\int_{S_q} f(x_i)dx_2dx_3 = \varepsilon^2 \int_{S_q} f(x_i, y_\alpha)dy_2dy_3$$

$$\text{and} \quad \int_{\partial S} f(x_i)dx_{\partial S} = \varepsilon \int_{\partial S} f(x_i, y_\alpha)dy_{\partial S}$$

Further, we adopt the following notations ($q = m, p$)

$$|S_q| = \int_{S_q} dS, \quad |S'_q| = \int_{S_q} ds = \varepsilon^{-2}|S_q|;$$

$$I_{q\alpha} = \int_{S_q} x_\alpha^2 dS, \quad I_{q\alpha\prime} = \int_{S_q} y_\alpha^2 ds = \varepsilon^{-4} I_{q\alpha}$$

and local problems are set on the "natural" y–frame originated at the beam section center of mass G and orientated along its principal inertia axis, so that

$$\int_{S_p} y_\alpha ds = 0 \quad \text{and} \quad \int_{S_p} y_\alpha y_\beta ds = 0 \quad \text{for} \quad \alpha \neq \beta.$$

2.2. Appropriate two-scale representation of dynamic balance equations

Note first that the specificity of the axial direction leads to decompose strain tensor $\underline{\underline{e}}$, and stress tensor $\underline{\underline{\sigma}}$ ($\underline{\underline{\sigma}} = \lambda \mathrm{tr}(\underline{\underline{e}})\underline{\underline{I}} + 2\mu\underline{\underline{e}}$) – that take the values ${}^q\underline{\underline{e}}$ and ${}^q\underline{\underline{\sigma}}$ in each constituent ($q = m, p$) – into three reduced tensors:

$$\underline{\underline{A}} = A_n \underline{a}_1 \otimes \underline{a}_1 + (\underline{A}_t \otimes \underline{a}_1 + \underline{a}_1 \otimes \underline{A}_t) + \underline{\underline{A}}_s,$$

where $\underline{\underline{A}} = \underline{\underline{e}}$ or $\underline{\underline{A}} = \underline{\underline{\sigma}}$

with:

- $A_n = A_{11}$: *scalar axial* strain or stress;
- $\underline{A}_t = A_{1\alpha}\underline{a}_\alpha$: 2D strain or stress *vector* exerted *out of the plane* of the section;
- $\underline{\underline{A}}_s = A_{\alpha\beta}/2(\underline{a}_\alpha \otimes \underline{a}_\beta + \underline{a}_\beta \otimes \underline{a}_\alpha)$: second rank *tensor* of the strain or stress *in the plane* of the section.

By using the two scale formulation, these tensors read (where $\underline{\underline{I}}_s = \underline{a}_2 \otimes \underline{a}_2 + \underline{a}_3 \otimes \underline{a}_3$):

$$e_n = u_{1,x_1}; \sigma_n = 2\mu e_n + \lambda(\mathrm{tr}(\underline{\underline{e}}_s) + e_n)$$

$$\underline{e}_t = [(\varepsilon^{-1}u_{1,y_\alpha} + u_{1,x_\alpha} + u_{\alpha,x_1})/2]\underline{a}_\alpha;\ \underline{\sigma}_t = 2\mu\underline{e}_t$$

$$\underline{\underline{e}}_s = \varepsilon^{-1}[(u_{\alpha,y_\beta} + u_{\beta,y_\alpha})/2](\underline{a}_\alpha \otimes \underline{a}_\beta + \underline{a}_\beta \otimes \underline{a}_\alpha)/2;$$

$$\underline{\underline{\sigma}}_s = 2\mu\underline{\underline{e}}_s + \lambda(\mathrm{tr}(\underline{\underline{e}}_s) + e_n)\underline{\underline{I}}_s$$

The beam and matrix dynamic equilibriums in harmonic regime read (as the problem is linear, the term $\exp(i\omega t)$ is omitted to lighten the notations):

$$\begin{cases} \underline{\mathrm{div}}({}^q\underline{\underline{\sigma}}) = -\rho_q\omega^{2q}\underline{u} & \text{in } S_q \\ [\underline{\underline{\sigma}}.\underline{n}] = \underline{0}, \quad [\underline{u}] = \underline{0} & \text{on } \Gamma; {}^m\underline{\underline{\sigma}} \quad S-\text{periodic in } \underline{y} \end{cases} \tag{1}$$

where $[.]$ denotes the jump at the interface. This set is rewritten with the two scale variables (x_i, y_α) and split into:

– scalar equations expressing the axial balance (along $\underline{a}_1$):

$$\begin{cases} \varepsilon^{-1}\mathrm{div}_y({}^q\underline{\sigma}_t) + \mathrm{div}_x({}^q\underline{\sigma}_t) + \frac{\partial^q\sigma_n}{\partial x_1} = -\rho_q\omega^{2q}u_1 \ \text{in} S_q,\ q=m,p \\ [\underline{\sigma}_t.\underline{n}] = 0,\ [u_1] = 0 \qquad \text{on} \Gamma; {}^m\underline{\sigma}_t\ S-\text{periodic in} \underline{y} \end{cases} \tag{2}$$

– vectorial sets expressing the in-plane balance (within $(\underline{a}_2, \underline{a}_3)$):

$$\begin{cases} \varepsilon^{-1}\underline{\mathrm{div}}_y({}^q\underline{\underline{\sigma}}_s) + \underline{\mathrm{div}}_x({}^q\underline{\underline{\sigma}}_s) + \frac{\partial^q\underline{\sigma}_t}{\partial x_1} = -\rho_q\omega^2 u_\alpha\underline{a}_\alpha \ \text{in} S_q,\ q=m,p \\ [\underline{\underline{\sigma}}_s.\underline{n}] = \underline{0},\ [u_\alpha\underline{a}_\alpha] = \underline{0} \qquad \text{on} \Gamma; {}^m\underline{\underline{\sigma}}_s\ S-\text{periodic in} \underline{y} \end{cases} \tag{3}$$

2.3. Scaling of stiffnesses and frequency

The contrast between the matrix and the reinforcement elastic properties plays a crucial role: without matrix, the beam lattice is governed by bending; if the matrix and the reinforcement material stiffnesses are identical, the behavior of the infinite composite layer is governed by shear. In particular, such a medium behaves as a generalized continuum - where both constituents contribute to the macroscopic behavior at the leading order - when the matrix elastic coefficients are two order smaller (in terms of ε power) than the beam ones (see e.g. Boutin and Soubestre, 2011). In dynamics, it has been demonstrated in Auriault and Bonnet (1985) that the same level of contrast leads to inner dynamic phenomena in stratified composites. That is why, in the sequel, we focus on media presenting a ε^2 stiffness contrast, i.e.:

$$\mu_m = O(\varepsilon^2\mu_p) \text{ and consequently } \lambda_m = O(\varepsilon^2\lambda_p)$$

To integrate this contrast in the asymptotic process, matrix elastic coefficients are rescaled by taking the beam ones as reference:

$$\mu_m = O(\varepsilon^2\mu_p) = \varepsilon^2\mu'_m \text{ with } \mu'_m = O(\mu_p)$$
$$\lambda_m = O(\varepsilon^2\lambda_p) = \varepsilon^2\lambda'_m \text{ with } \lambda'_m = O(\lambda_p)$$

and the stresses in both constituents are written in the form below:

$${}^p\underline{\underline{\sigma}} = \lambda_p\mathrm{tr}({}^p\underline{\underline{e}})\underline{\underline{I}} + 2\mu_p\,{}^p\underline{\underline{e}} \quad {}^m\underline{\underline{\sigma}} = \varepsilon^2\left(\lambda'_m\mathrm{tr}({}^m\underline{\underline{e}})\underline{\underline{I}} + 2\mu'_m\,{}^m\underline{\underline{e}}\right) \tag{4}$$

A dynamic regime of characteristic macroscopic length L, may either involve the beam compression dynamics or a dynamic regime within the matrix. Both phenomena are associated with a characteristic angular frequency:

$$\omega_p = \sqrt{\frac{E_p}{\rho_p}}\frac{1}{L}; \quad \omega_m = \sqrt{\frac{\mu_m}{\rho_m}}\frac{1}{L}$$

With densities ρ_p and ρ_m of the same order of magnitude, the ratio ω_m/ω_p is then of the order of magnitude of the square root of the stiffness contrast:

$$\frac{\omega_m}{\omega_p} = \sqrt{\frac{\rho_p\mu_m}{\rho_m E_p}} = O\left(\sqrt{\frac{\mu_m}{\mu_p}}\right) = O(\varepsilon)$$

It leads us to identify different frequency ranges of interest:

- $\omega \leqslant \varepsilon^2 O(\omega_p) = \varepsilon O(\omega_m)$. In that case, the characteristic wavelengths λ_p and λ_m associated with both mechanisms are significantly large compared to the reinforced medium macroscopic size L

$$\frac{\lambda_p}{2\pi} = \sqrt{\frac{E_p}{\rho_p}}\frac{1}{\omega} \geqslant \varepsilon^{-2}L \gg L; \ \frac{\lambda_m}{2\pi} = \sqrt{\frac{\mu_m}{\rho_m}}\frac{1}{\omega} \geqslant \varepsilon^{-1}L \gg L$$

Hence, inertia effects related to both mechanisms are negligible and therefore the whole system is in a quasi-static regime.

- $\omega = \varepsilon O(\omega_p) = O(\omega_m)$. The characteristic wavelengths are then assessed as

$$\frac{\lambda_p}{2\pi} = \sqrt{\frac{E_p}{\rho_p}}\frac{1}{\omega} = \varepsilon^{-1}L; \quad \frac{\lambda_m}{2\pi} = \sqrt{\frac{\mu_m}{\rho_m}}\frac{1}{\omega} = L$$

Therefore, a macroscopic dynamics arises within the reinforced medium. Such a regime involves the macro-dynamics of the matrix while the beam compression mechanism remains in a quasi-static regime.

- $\omega = O(\omega_p) = \varepsilon^{-1}O(\omega_m)$. It implies that:

$$\frac{\lambda_p}{2\pi} = \sqrt{\frac{E_p}{\rho_p}}\frac{1}{\omega} = L; \quad \frac{\lambda_m}{2\pi} = \sqrt{\frac{\mu_m}{\rho_m}}\frac{1}{\varepsilon^{-1}\omega} = \varepsilon L = l$$

Thus, another macroscopic dynamic regime is expected within the reinforced medium. This particular regime involves the beam compression macro-dynamics and the dynamic phenomenon at the scale of the period in the matrix. At higher frequencies (i.e. $\omega \geqslant \varepsilon^{-1}O(\omega_p)$) no phenomenon presents a scale separation and those situations cannot be described through homogenization. The different regimes (quasi-static, macro-dynamic, local-dynamic, non-homogenizable) for both mechanisms are represented in Fig. 3 according to the angular frequency.

To study these different possibilities, the angular frequency, hence inertial terms, is rescaled by taking ω_p as reference, that is:

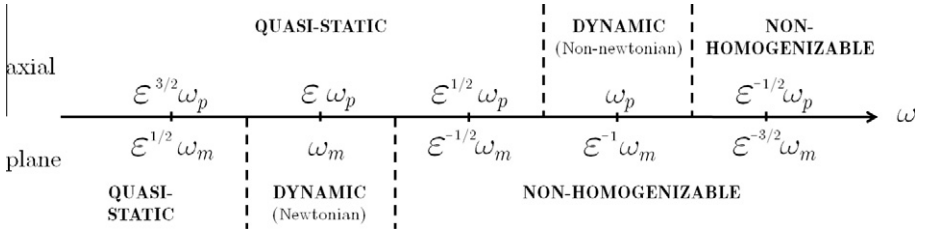

Fig. 3. Macroscopic behavior domains as a function of the angular frequency for a two order stiffness contrast reinforced medium ($\mu_m = O(\varepsilon^2\mu_p)$).

$$\omega = \varepsilon^{w/2}\omega', \text{ then } -\rho_q\omega^{2q}\underline{u} = -\rho_q\varepsilon^w\omega'^{2q}\underline{u} \quad \text{with} \quad \omega' = O(\omega_p) \tag{5}$$

and the cases $w > 2$, $w = 2$, and $w = 0$ enable to go through quasi-static states (Section 3) to dynamic states (Section 4).

2.4. Asymptotic expansions and series of local problems

Finally, according to the asymptotic process, motions in both constituents ($q = m, p$) are looked for in the form of two-scale expansions in powers of ε:

$$^q\underline{u} = \sum_{k=0}^{\infty}\varepsilon^k({}^q u_j^k(x_i, y_\alpha)\underline{a}_j)$$
$$\text{with} \quad {}^m u_j^k(x_i, y_\alpha) \quad S-\text{periodic in } y_\alpha.$$

Thereby, the reduced strain tensors expansions are:

$$\begin{aligned}
&{}^q\mathrm{e}_{\mathrm{n}} = \sum_{k=0}^{\infty}\varepsilon^k\,{}^q\mathrm{e}_{\mathrm{n}}^k \quad \text{with} \quad {}^q\mathrm{e}_{\mathrm{n}}^k = \frac{\partial u_1^k}{\partial x_1}\\
&{}^q\underline{\mathrm{e}}_{\mathrm{t}} = \sum_{k=-1}^{\infty}\varepsilon^k\,{}^q\underline{\mathrm{e}}_{\mathrm{t}}^k \quad \text{with} \quad {}^q\underline{\mathrm{e}}_{\mathrm{t}}^k = \frac{1}{2}\left(\frac{\partial u_1^{k+1}}{\partial y_\alpha} + \frac{\partial u_1^k}{\partial x_\alpha} + \frac{\partial u_\alpha^k}{\partial x_1}\right)\underline{a}_\alpha\\
&{}^q\underline{\underline{\mathrm{e}}}_{\mathrm{s}} = \sum_{k=-1}^{\infty}\varepsilon^k\,{}^q\underline{\underline{\mathrm{e}}}_{\mathrm{s}}^k \quad \text{with} \quad {}^q\underline{\underline{\mathrm{e}}}_{\mathrm{s}}^k = \underline{\underline{\mathrm{e}}}_{ys}(\underline{u}^{k+1}) + \underline{\underline{\mathrm{e}}}_{xs}(\underline{u}^k)
\end{aligned} \tag{6}$$

and reporting those expressions into (4) provides the reduced stress tensors expansions. For example:

$${}^p\underline{\underline{\sigma}}_s = \sum_{k=-1}^{\infty}\varepsilon^k\,{}^p\underline{\underline{\sigma}}_s^k \quad \text{with} \quad {}^p\underline{\underline{\sigma}}_s^k = \lambda_p(\mathrm{div}_x(\underline{u}^k) + \mathrm{div}_y(\underline{u}^{k+1}))\underline{\underline{\mathrm{I}}}_s + 2\mu_p\,{}^p\underline{\underline{\mathrm{e}}}_s^k$$

$$\begin{aligned}
&{}^m\underline{\underline{\sigma}}_s = \sum_{k=1}^{\infty}\varepsilon^k\,{}^m\underline{\underline{\sigma}}_s^k\\
&{}^m\underline{\underline{\sigma}}_s^k = \lambda'_m(\mathrm{div}_x(\underline{u}^{k-2}) + \mathrm{div}_y(\underline{u}^{k-1}))\underline{\underline{\mathrm{I}}}_s + 2\mu'_m\,{}^m\underline{\underline{\mathrm{e}}}_s^{k-2}
\end{aligned} \tag{7}$$

In both constituents, local problems at different orders are obtained by introducing the asymptotic expansions of rescaled stress (e.g. (7)) into the dynamic balance equations (2) and (3) which are rescaled with (5). Then, local problems are solved successively (by increasing the ε power) until the macroscopic description is obtained.

Remark: As we focus on the leading order description, the angular frequency is not expanded. Then ω used herein represents either the actual frequency when studying the forced harmonic vibration, or the first order of the expansion ($\omega = \omega^0$) when studying the dynamic response or under given boundary conditions.

3. Quasi-static homogenized model

Let us first focus on the quasi-static description reached when considering $\omega \leqslant \varepsilon O(\omega_m)$, i.e. $w > 2$ in (5). Since this situation is similar to the homogenization of a "soft" elastic material periodically reinforced by "stiff" linear slender elastic inclusions already treated in Boutin and Soubestre (2011), we restrict the presentation to the main steps necessary for the sequel of the study.

3.1. Beam

Due to the stiffness contrast, the two first problems concern the beam only, as in absence of matrix. Thus, one obtains a solution close to the classic solution of Euler–Bernoulli beams, that is (capital variables are independent of y_α):

$$\begin{aligned}
&{}^p\underline{u}^0 = \underline{U}^0(\underline{x})\\
&{}^p\underline{u}^1 = -2(\underline{\mathrm{e}}_{xt}(\underline{U}^0).\underline{y})\underline{a}_1 - \nu_p\frac{\partial U_1^0}{\partial x_1}\underline{y} - \underline{\mathrm{e}}_{xs}(\underline{U}^0).\underline{y}\\
&\qquad + {}^p\Theta^0(\underline{x})\underline{a}_1 \wedge \underline{y} + \underline{U}^1(\underline{x})\\
&{}^p\underline{\underline{\mathrm{e}}}^0 = \frac{\partial U_1^0}{\partial x_1}\left[\underline{a}_1 \otimes \underline{a}_1 - \nu_p\underline{\underline{I}}_s\right]; \quad {}^p\underline{\underline{\sigma}}^0 = E_p\frac{\partial U_1^0}{\partial x_1}[\underline{a}_1 \otimes \underline{a}_1]
\end{aligned}$$

The leading order motion is a rigid translation $\underline{U}^0$ of the section. The first order motion ${}^p\underline{u}^1$ consists in

- an axial component split into a rigid axial translation $U_1^1\underline{a}_1$ and an axial term related to the tangential strain $\underline{\mathrm{e}}_{xt}(\underline{U}^0)$ that expresses the out-of-plane rotation of the section,
- in-plane components decomposed into, (i) a rigid in-plane translation $U_\alpha^1\underline{a}_\alpha$ and rotation ${}^p\Theta^0$ of the beam section (note that the actual torsion of the beam ${}^p\Omega^0$ is obtained by substracting the material rotation, i.e. ${}^p\Omega^0 = {}^p\Theta^0 - (\partial U_2^0/\partial x_3 - \partial U_3^0/\partial x_2)/2$), (ii) the Poisson effect induced by the macro-compression $\frac{\partial U_1^0}{\partial x_1}$, (iii) the "local compensation" of the macro in-plane deformation $\underline{\underline{\mathrm{e}}}_{xs}(\underline{U}^0)$.

Finally, strain and stress tensors at the leading order correspond to a non-uniform state of simple compression (or traction).

3.2. Matrix

Knowing the beam motion at the two first orders enables to treat the two Dirichlet problems governing the matrix equilibrium with continuity of motion with the beam. At the leading order the matrix motion ${}^m\underline{u}^0$ is governed by:

$$\begin{cases} \underline{\mathrm{div}}_y({}^m\underline{\underline{\sigma}}^1) = \underline{0} & \text{in } S_m \\ {}^m\underline{u}^0 = \underline{U}^0 & \text{on } \Gamma; \quad {}^m\underline{u}^0 \ S-\text{periodic in } y \end{cases}$$

Obviously, the matrix follows the uniform translation imposed by the beam section, so that there is a global beam-matrix translation, and that the associated stress tensor is null:

$${}^m\underline{u}^0 = \underline{U}^0(x_i); \qquad {}^m\underline{\underline{\sigma}}^1 = \underline{\underline{0}}$$

At the following order, the equations enabling the determination of ${}^m\underline{u}^1$ and ${}^m\underline{\underline{\sigma}}^2$ express the equilibrium of the matrix subjected on Γ to the motion and the deformation of the beam section:

$$\begin{cases} \underline{\mathrm{div}}_y({}^m\underline{\underline{\sigma}}^2) = \underline{0} \text{ in } S_m \\ {}^m\underline{\underline{\sigma}}^2 = \lambda'_m\left(\mathrm{div}_y({}^m\underline{u}^1) + \mathrm{div}_x(\underline{U}^0)\right)\underline{\underline{I}} + 2\mu'_m\left(\underline{\underline{e}}_y({}^m\underline{u}^1) + \underline{\underline{e}}_x(\underline{U}^0)\right) \\ {}^m\underline{u}^1 = {}^p\underline{u}^1 \text{ on } \Gamma; \quad {}^m\underline{u}^1 \ \ S-\text{periodic in } y \end{cases} \tag{8}$$

By linearity, as in usual homogenization of composites, the solution ${}^m u^1$ is the sum of terms depending on the macroscopic strain tensor $\underline{\underline{e}}_x(\underline{U}^0)$ components and of a uniform translation $\underline{U}^1$. Hence, the stress tensor is in the form ${}^m\underline{\underline{\sigma}}^2 = \underline{\underline{\underline{\underline{c}}}}'(\underline{y}) : \underline{\underline{e}}_x(\underline{U}^0)$, or ${}^m\sigma^2_{ij} = c'^{kl}_{ij}e_{xkl}(\underline{U}^0)$, where $c'^{ii}_{1\alpha} = c'^{23}_{1\alpha} = c'^{1\alpha}_{ii} = c'^{1\alpha}_{23} = 0$ due to the 2D geometry of the period (see Appendix).

3.3. Beam and Matrix

Now, let us come back to the beam equilibrium together with the stress continuity on the interface. Fields ${}^p\underline{u}^2$ and ${}^p\underline{\underline{\sigma}}^1$ satisfy the following Neumann problem:

$$\begin{cases} \frac{\partial {}^p\sigma^0_n}{\partial x_1}\underline{a}_1 + \underline{\mathrm{div}}_y({}^p\underline{\underline{\sigma}}^1) = \underline{0} \text{ in } S_p \\ {}^p\underline{\underline{\sigma}}^1 = \lambda_p\left(\mathrm{div}_x({}^p\underline{u}^1) + \mathrm{div}_y({}^p\underline{u}^2)\right)\underline{\underline{I}} + 2\mu_p\left(\underline{\underline{e}}_y({}^p\underline{u}^2) + \underline{\underline{e}}_x({}^p\underline{u}^1)\right) \\ {}^p\underline{\underline{\sigma}}^1 \cdot \underline{n} = \underline{0} \text{ on } \Gamma \end{cases} \tag{9}$$

Through the integration over S_p of this balance equation, the use of the divergence theorem and the Neumann condition, one deduces the macroscopic axial equilibrium at the leading order:

$$\frac{\partial}{\partial x_1}\int_{S_p} {}^p\sigma^0_n ds = 0 \tag{10}$$

Then, the resolution shows that ${}^p\underline{u}^2$ is the sum of:

- a rigid body motion composed by a plane rotation ${}^p\Theta^1$ and a uniform translation ${}^p\underline{U}^2$,
- terms induced by the second gradient of $\underline{U}^0$ and by the gradient of ${}^p\Theta^0$ and of $\underline{U}^1$.

Furthermore, diagonal and tangential components appear in ${}^p\underline{\underline{e}}^1$ and ${}^p\underline{\underline{\sigma}}^1$ and we have ${}^p\underline{\underline{\sigma}}^1_s = \underline{\underline{0}}$, $\int_{S_p} {}^p\underline{\sigma}^1_t ds = \underline{0}$ and $\int_{S_p} {}^p\underline{\sigma}^1_t . \underline{y} ds = 0$ (see Appendix).

At the next order, the global equilibrium of the beam/matrix composite is described by

$$\begin{cases} \underline{\mathrm{div}}_x({}^p\underline{\underline{\sigma}}^1) + \underline{\mathrm{div}}_y({}^p\underline{\underline{\sigma}}^2) = \underline{0} & \text{in } S_p \\ \underline{\mathrm{div}}_y({}^m\underline{\underline{\sigma}}^2) = \underline{0} & \text{in } S_m \\ [\underline{\underline{\sigma}}^2 . \underline{n}] = \underline{0} & \text{on } \Gamma; \quad {}^m\underline{\underline{\sigma}}^2 \ S-\text{periodic in } y \end{cases} \tag{11}$$

On the one hand, the integration over S_m and S_p of the matrix and beam axial equilibriums with the usual integral transformations and the properties of ${}^p\underline{\sigma}^1_t$, provides the macroscopic axial equilibrium at the first order:

$$\frac{1}{|S'|}\frac{\partial}{\partial x_1}\int_{S_p} {}^p\sigma^1_n ds = 0 \tag{12}$$

On the other hand, taking the product by $\underline{y}$ of the axial equilibrium within the two constituents and integrating over S_m and S_p leads, after some algebra, to the mean value of tangential stresses on the period $\langle \underline{\sigma}^2_t \rangle$ (where $\langle . \rangle$ stands for $(\int_{S_p} ds + \int_{S_m} ds)/|S'|$). Moreover, taking the tensorial product by $\underline{y}$ of the in-plane equilibrium within the two constituents and integrating over S_m and S_p leads to the mean value of in-plane stresses $\langle \underline{\underline{\sigma}}^2_s \rangle$. And finally, the resolution gives the mean value of the mean axial stress $\langle \sigma^2_n \rangle$. The complete expression of $\langle \underline{\underline{\sigma}}^2 \rangle$ is given below in equation (14).

To close the macroscopic description, it remains to consider the equilibrium at the following order

$$\begin{cases} \underline{\mathrm{div}}_x({}^m\underline{\underline{\sigma}}^2) + \underline{\mathrm{div}}_y({}^m\underline{\underline{\sigma}}^3) = \underline{0} & \text{in } S_m \\ \underline{\mathrm{div}}_x({}^p\underline{\underline{\sigma}}^2) + \underline{\mathrm{div}}_y({}^p\underline{\underline{\sigma}}^3) = \underline{0} & \text{in } S_p \\ [\underline{\underline{\sigma}}^3 . \underline{n}] = \underline{0} & \text{on } \Gamma; \quad {}^m\underline{\underline{\sigma}}^3 \ S-\text{periodic in } y \end{cases} \tag{13}$$

The integration over S_m and S_p of both equilibriums yields the macroscopic equilibrium of the beam/matrix composite:

$$\underline{\mathrm{div}}_x(\langle \underline{\underline{\sigma}}^2 \rangle) = \underline{0}$$

3.4. Macroscopic description

To sum up, after coming back to the global motion $\underline{U}^0(\underline{x}) + \underline{\widetilde{U}}^2(\underline{x}) + \cdots = \underline{U}^0(\underline{x}) + \varepsilon^2\underline{U}^2(\underline{x}) + \cdots$, the physical mean stresses $\langle \underline{\underline{\sigma}}^0 \rangle + \langle \underline{\underline{\widetilde{\sigma}}}^2 \rangle = \langle \underline{\underline{\sigma}}^0 \rangle + \varepsilon^2 \langle \underline{\underline{\sigma}}^2 \rangle$, and the unscaled elastic and geometric parameters, the macroscopic behavior is described by the following macroscopic equilibriums and constitutive laws at the orders ε^0 and ε^2 (the expressions of the macroscopic elastic tensor $\underline{\underline{\underline{\underline{C}}}}$ - that is transverse isotropic for bi-symmetric matrix/beam section - and of $\mathcal{J}_{p\alpha}$ are given in the Appendix):

$$\underline{\mathrm{div}}_x(\langle\underline{\underline{\sigma}}^0\rangle)=\underline{0};\quad \left\langle\underline{\underline{\sigma}}^0\right\rangle=E_p\frac{|S_p|}{|S|}\frac{\partial U_1^0}{\partial x_1}\underline{a}_1\otimes\underline{a}_1$$

$$\underline{\mathrm{div}}_x(\langle\underline{\underline{\tilde{\sigma}}}^2\rangle)=\underline{0};\quad \langle\underline{\underline{\tilde{\sigma}}}^2\rangle=\underline{\underline{\underline{C}}}:\underline{\underline{e}}_x(\underline{U}^0)+E_p\frac{|S_p|}{|S|}\frac{\partial^p\tilde{U}_1^2}{\partial x_1}\underline{a}_1\otimes\underline{a}_1$$
$$+\frac{E_p}{|S|}\left(\nu_p\frac{(I_{p2}+I_{p3})}{2}\frac{\partial^3U_1^0}{\partial x_1^3}+\frac{I_{p\alpha}}{2}\left(\frac{\partial^3U_1^0}{\partial x_1\partial x_\alpha^2}+2\frac{\partial^3U_\alpha^0}{\partial x_1^2\partial x_\alpha}\right)\right)\underline{a}_1\otimes\underline{a}_1$$
$$+\left(-E_p\frac{I_{p\alpha}}{|S|}\left(\frac{\partial^3U_1^0}{\partial x_1^2\partial x_\alpha}+\frac{\partial^3U_\alpha^0}{\partial x_1^3}\right)+\mu_p\frac{\mathcal{J}_{p\alpha}}{|S|}\frac{\partial^2{}^p\Omega^0}{\partial x_1\partial x_{\overline{\alpha}}}\right)(\underline{a}_1\otimes\underline{a}_\alpha+\underline{a}_\alpha\otimes\underline{a}_1)\tag{14}$$

According to the frequency range ($\omega\leqslant\varepsilon O(\omega_m)$, i.e. $w>2$) no dynamic effect appears and the above description corresponds to a quasi-static state.

Note that $\underline{U}^1$ is disregarded without restriction since its governing equation is identical to the one governing $\underline{U}^0$ (hence $\underline{U}^1$ can be added to $\underline{U}^0$). For generality, the term related to the beam torsion ${}^p\Omega^0$ is kept. However, this kinematics, independent of the translation, would require a specific action on each beam and is not considered in the sequel.

Due to the stiffness contrast and the parallel orientation of the beams, the behavior is strongly linked to the type of kinematics. This is evidenced by splitting the leading order motion $\underline{U}^0$ into its transverse part $U_\alpha^0\underline{a}_\alpha$ and its axial part $U_1^0\underline{a}_1$:

Transverse motions $U_\alpha^0(\underline{x})\underline{a}_\alpha$.

- if the transverse motion is independent of the axial variable, i.e. $U_\alpha^0=U_\alpha^0(x_\beta\underline{a}_\beta)$: the medium behaves as a classical composite governed by the "in-plane reduction" of $\underline{\underline{\underline{C}}}$ (which is of the order of μ_m),
- if the transverse motion only depends on the axial variable, i.e. $U_\alpha^0=U_\alpha^0(x_1)$: the medium behaves as a *second gradient continuum at the leading order*. Noteworthy, the mechanisms of shear of the matrix and bending of the beam ($\partial^3U_\alpha^0/\partial x_1^3$) contribute to the mean stress at the same order,
- if the transverse motion depends on both axial and in-plane variables, i.e. $U_\alpha^0=U_\alpha^0(\underline{x})$: the medium also behaves as a second gradient continuum. In addition to the bending of the beam, the second gradient of the deformation involves axial effects due to inhomogeneous kinematics of in-plane confinement ($\partial^3U_\alpha^0/\partial x_1^2\partial x_\alpha$). As a consequence of the axial equilibrium requirement, an axial motion of two order smaller $\tilde{U}_1^2(\underline{x})\underline{a}_1$ arises as a corrector.

Axial motions $U_1^0(\underline{x})\underline{a}_1$.

- if the axial motion is independent of the axial variable, i.e. $U_1^0=U_1^0(x_\beta\underline{a}_\beta)$: the medium behaves as a classical composite governed by the "$(\underline{a}_1,\underline{a}_\alpha)$ reduction" of $\underline{\underline{\underline{C}}}$,
- if the axial motion just depends on the axial variable, i.e. $U_1^0=U_1^0(x_1)$: the material behaves at the leading order as a highly anisotropic elastic medium governed by the compression of the beams (of the order of E_p). Considering order ε^2, a corrector $\tilde{U}_1^2(x_1)\underline{a}_1$ appears to balance the axial gradient of Poisson effects and the compression in the matrix. Hence, conversely to transverse motions, the second gradient continuum only appears as a corrector,
- if the axial motion depends on both axial and in-plane variables, i.e. $U_1^0=U_1^0(\underline{x})$: we observe a similar behavior as for $U_1^0(x_1)\underline{a}_1$ except that the corrector $\tilde{U}_1^2(x_1)\underline{a}_1$ also balances axial and transverse effects due to inhomogeneous kinematics of compression ($\partial^3U_1^0/\partial x_1\partial x_\alpha\partial x_i$).

In presence of a second gradient effect at the leading order, the usual leading order boundary conditions, expressed in terms of mean stress and motion, have to be completed by conditions relative to the momentum and the rotation of the beam (in accordance with the actual conditions imposed to the fibers). This point is detailed in Section 5.

4. Dynamic homogenized model

In this Section, the different dynamic macroscopic behaviors of an ε^2-contrast reinforced medium are examined considering successively the two frequency ranges $\omega=\varepsilon O(\omega_p)=O(\omega_m)$ (i.e. $w=2$ in (5)) and then $\omega=O(\omega_p)=\varepsilon^{-1}O(\omega_m)$ (i.e. $w=0$ in (5)). It is shown that these two frequency ranges respectively correspond to the macroscopic transverse and axial dynamics. The dynamic homogenized models are derived in the same way as for the quasi-static modelling, except that inertial terms appear at increasing orders.

4.1. Transverse dynamic behavior: $\omega=\varepsilon O(\omega_p)=O(\omega_m)$

In this frequency range, the inertial term is of order two ($w=2$ in (5)). Hence, all problems solved in the quasi-static state remain unchanged until the last closure problem (Section 3.3) in which the inertia effect emerges. As the previous problems (and then their solutions) are not modified, the leading order stress state and the related balance equation (10) still apply, therefore:

$$\underline{\mathrm{div}}_x(\langle\underline{\underline{\sigma}}^0\rangle)=\underline{0};\quad \left\langle\underline{\underline{\sigma}}^0\right\rangle=E_p\frac{|S_p|}{|S|}\frac{\partial U_1^0}{\partial x_1}\underline{a}_1\otimes\underline{a}_1\tag{15}$$

Equations (15) give the axial equilibrium at the leading order. The absence of inertia terms evidences that the axial regime remains in a quasi-static state. Now, observing that the expression of $\langle\underline{\underline{\tilde{\sigma}}}^2\rangle$ given in 14 is also unchanged, and noting that the leading order dynamic term reads $-\rho_q\omega^2\underline{U}^0=-\rho_q\varepsilon^2\omega'^2\underline{U}^0$, the closure problem (13) becomes:

$$\begin{cases}\underline{\mathrm{div}}_x({}^m\underline{\underline{\sigma}}^2)+\underline{\mathrm{div}}_y({}^m\underline{\underline{\sigma}}^3)=-\rho_m\omega'^2\underline{U}^0 & \text{in } S_m\\ \underline{\mathrm{div}}_x({}^p\underline{\underline{\sigma}}^2)+\underline{\mathrm{div}}_y({}^p\underline{\underline{\sigma}}^3)=-\rho_p\omega'^2\underline{U}^0 & \text{in } S_p\\ [\underline{\underline{\sigma}}^3.\underline{n}]=\underline{0}\ \text{ on } \Gamma;\ {}^m\underline{\underline{\sigma}}^3\ \ S-\text{periodic in } y\end{cases}\tag{16}$$

Integrating both equilibriums, then coming back to the usual variables, one obtains the macroscopic dynamics of the beam/matrix composite:

$$\underline{\mathrm{div}}_x(\langle\underline{\underline{\tilde{\sigma}}}^2\rangle)=-\langle\rho\rangle\omega^2\underline{U}^0\tag{17}$$

By focusing on translation kinematics (without the independent beam torsion i.e. ${}^{p}\Omega^0 = 0$), and since (15) imposes that $\frac{\partial^2 U_1^0}{\partial x_1^2} = 0$, the expression of $\langle \widetilde{\underline{\underline{\sigma}}}^2 \rangle$ is simplified. Then, one extracts from (17) the following leading order in-plane balance equations that were missed at the previous order (where $\{ij\} = \{11, 22, 33, 23\}$):

$$\underline{\mathrm{div}}_x\left(\langle \widetilde{\underline{\sigma}}_{\mathrm{t}}^2 \rangle \otimes \underline{a}_1 + \langle \widetilde{\underline{\underline{\sigma}}}_{s}^2 \rangle\right) = -\langle \rho \rangle \omega^2 U_\alpha^0 \underline{a}_\alpha$$

$$\langle \widetilde{\underline{\sigma}}_{\mathrm{t}}^2 \rangle \otimes \underline{a}_1 + \langle \widetilde{\underline{\underline{\sigma}}}_{s}^2 \rangle = \left(C_{1\alpha}^{1\beta} \mathbf{e}_{x1\beta}(\underline{U}^0) - E_p \frac{I_{p\alpha}}{|S|} \frac{\partial^3 U_\alpha^0}{\partial x_1^3} \right) \underline{a}_\alpha \otimes \underline{a}_1 + C_{\alpha\beta}^{ij} \mathbf{e}_{xij}(\underline{U}^0) \underline{a}_\alpha \otimes \underline{a}_\beta \tag{18}$$

This set expresses the dynamics associated with the transverse kinematics. A second gradient effect is involved at the leading order when the transverse component U_α presents an x_1-axial variation (that induces inner bending). Note that the elastic parameters identified in the quasi-static regime remain unchanged. As for inertia, the equivalent density is the mean density as in classic dynamics of elastic composites. The specificity of the transverse dynamics with second gradient effect is studied in Section 5.1.

Remark: The axial balance included in (17) is the second order corrector of (15) and governs the axial corrector $\widetilde{U}_1^2$ of the motion. Thus, a slight ε^2-dynamic effect exists in the axial direction.

4.2. Axial dynamic behavior: $\omega = O(\omega_p) = \varepsilon^{-1} O(\omega_m)$

Let us consider the higher frequency range $\omega = O(\omega_p) = \varepsilon^{-1} O(\omega_m)$. Here, the inertial term is of order zero ($w = 0$ in (5) thus $\omega' = \omega$). Consequently, only the first and second problems of the quasi-static case defining the beam motions at the two first orders (Section 3.1) remain unmodified.

However, at the leading order, the matrix now undergoes a dynamic regime, and the motion ${}^{m}\underline{u}^0$ is governed by the following set, with Dirichlet conditions:

$$\begin{cases} \underline{\mathrm{div}}_y({}^{m}\underline{\underline{\sigma}}^1) = -\rho_m \omega^2 \, {}^{m}\underline{u}^0 & \text{in } S_m \\ {}^{m}\underline{u}^0 = \underline{U}^0 & \text{on } \Gamma;\ {}^{m}\underline{u}^0 \quad S-\text{periodic in } y \end{cases}$$

As the matrix is elastic isotropic and because of the in-plane y dependence, this differential set can be split into two *independent* sets expressing the axial balance (related to ${}^{m}u_1^0$)

$$\begin{cases} \mu_m' \Delta_y({}^{m}u_1^0) = -\rho_m \omega^2 \, {}^{m}u_1^0 & \text{in } S_m \\ {}^{m}u_1^0 = U_1^0 & \text{on } \Gamma;\ {}^{m}u_1^0 \quad S-\text{periodic in } y \end{cases} \tag{19}$$

and the in-plane balance (related to ${}^{m}u_\alpha^0 \underline{a}_\alpha$):

$$\begin{cases} \lambda_m' \underline{\mathrm{grad}}_y(\mathrm{div}_y({}^{m}u_\alpha^0 \underline{a}_\alpha)) + \mu_m' \Delta_y({}^{m}u_\alpha^0 \underline{a}_\alpha) = -\rho_m \omega^2 {}^{m}u_\alpha^0 \underline{a}_\alpha & \text{in } S_m \\ {}^{m}u_\alpha^0 \underline{a}_\alpha = U_\alpha^0 \underline{a}_\alpha & \text{on } \Gamma;\ {}^{m}u_\alpha^0 \underline{a}_\alpha \quad S\text{-periodic in } y \end{cases} \tag{20}$$

By linearity, the solutions of these dynamic problems read

$${}^{m}u_1^0 = \zeta^1(\omega, y_2, y_3) U_1^0; \quad {}^{m}u_\alpha^0 \underline{a}_\alpha = \underline{\zeta}^\alpha(\omega, y_2, y_3) U_\alpha^0$$

where the *frequency dependent* scalar field $\zeta^1(\omega, y_2, y_3)$ and the vectorial fields $\underline{\zeta}^\alpha(\omega, y_2, y_3)$ are respectively the particular solutions of (19) and (20) for unit vertical and in-plane beam motions respectively.

Let us now establish the beam/matrix equilibrium. By noticing that the leading order inertia terms within the beam and the matrix are respectively $-\rho_p \varepsilon^0 \omega^2 \underline{U}^0$ and $-\rho_m \varepsilon^0 \omega^2 \underline{u}_m^0$, the governing equation in each constituent is:

$$\begin{cases} \underline{\mathrm{div}}_x({}^{p}\underline{\underline{\sigma}}^0) + \underline{\mathrm{div}}_y({}^{p}\underline{\underline{\sigma}}^1) = -\rho_p \omega^2 \underline{U}^0 & \text{in } S_p \\ \underline{\mathrm{div}}_y({}^{m}\underline{\underline{\sigma}}^1) = -\rho_m \omega^2 \, {}^{m}\underline{u}^0 & \text{in } S_m \\ [\underline{\underline{\sigma}}^1 . \underline{n}] = \underline{0} & \text{on } \Gamma;\ {}^{m}\underline{\underline{\sigma}}^1 \quad S-\text{periodic in } y \end{cases} \tag{21}$$

Integrating both equations provides:

- the axial macroscopic equilibrium and constitutive law of the reinforced medium:

$$\frac{\partial \langle \sigma_{\mathrm{n}}^0 \rangle}{\partial x_1} = -\langle \rho^* \rangle \omega^2 U_1^0 \text{ where } \langle \rho^* \rangle(\omega) = \frac{1}{|S|}\left(\rho_p |S_p| + \rho_m \int_{S_m} \zeta^1 dS\right)$$
$$\langle \sigma_{\mathrm{n}}^0 \rangle = E_p \frac{|S_p|}{|S|} \frac{\partial U_1^0}{\partial x_1} \tag{22}$$

- the in-plane balance condition

$$0 = -\frac{1}{|S|}\left(\rho_p |S_p| \delta_\beta^\alpha + \rho_m \int_{S_m} \zeta_\beta^\alpha dS\right) \omega'^2 U_\beta^0$$

Note that the in-plane balance condition imposes $U_\alpha^0 \underline{a}_\alpha = \underline{0}$. Indeed, in general the transverse inertia *tensor* does not vanish ($\rho_p |S_p| \delta_\beta^\alpha + \rho_m \int_{S_m} \zeta_\beta^\alpha dS \neq 0$ except possibly on a discrete frequency spectrum). Therefore, in this frequency range we have:

$$\underline{U}^0 = U_1^0 \underline{a}_1$$

Consequently, the description reduces to the *axial* macroscopic equilibrium (22). The salient feature of this latter is that the density is not the mean density $\langle \rho \rangle$ but an apparent density $\langle \rho^* \rangle(\omega)$ that depends on the frequency through $\zeta^1(\omega)$. The axial regime is characterized by the coexistence of a global dynamic regime carried by the beam vibrating axially and of an internal dynamic regime induced in the matrix undergoing a forced vibration state. This situation matches the concept of "metamaterial" evidenced in the pioneer paper by Auriault and Bonnet (1985) on periodically stratified composite media with high stiffness contrast and investigated in particular reinforced media by Vasseur et al. (1998). The apparent loss of the Newton law at the macroscale arises from the non equilibrium local state in the matrix, that results in turn in the non-uniform local motion. In the time domain, the macro dynamics involves a convolution product whose characteristic time is related to the resonance of the matrix. Hence, the macroscopic axial behavior of the reinforced medium has a non-local time response.

4.3. Feature of the "apparent" density $\langle\rho^*\rangle(\omega)$

For a given period geometry, the resolution of (19) at each frequency enables the determination of ζ^1 (for $U_1^0=1$) and then of $\langle\rho^*\rangle(\omega)$. As ζ^1 is determined by the elasto-dynamic problem (19) set in the matrix with a combination of Dirichlet and periodic boundary conditions, the properties of $\langle\rho^*\rangle$ are intrinsically related to the inner eigen modes associated with the resonance of the matrix in the period under these imposed boundary conditions. This is detailed hereafter, where, for convenience, we introduce

$$\zeta(\omega,\underline{y})=-1+\zeta^1(\omega,\underline{y})$$

so that the boundary value problem (19) becomes

$$\begin{cases}\mu'_m\Delta_y(\zeta)=-\rho_m\omega^2(1+\zeta) & \text{in } S_m\\ \zeta=0 & \text{on } \Gamma;\quad \zeta\ S\text{-periodic in } y\end{cases}$$

Similarly to Auriault and Bonnet (1985), let us consider the associated eigenvalue problem:

$$\begin{cases}\mu'_m\Delta_y(\phi)=-\lambda\phi & \text{in } S_m\\ \phi=0 & \text{on}\Gamma;\quad \phi\ S\text{-periodic in } y\end{cases}$$

By following Courant and Hilbert (1970), this problem has a discrete and positive spectrum

$$0\leqslant\lambda_1\leqslant\lambda_2\leqslant\lambda_3\leqslant\cdots$$

Each eigenvalue λ_J is associated with an eigenfunction ϕ^J and they correspond respectively to the resonance frequency of the matrix with the imposed boundary conditions, and to the associated modes shapes (here and in the sequel, capital indices are related to inner eigen mode of the matrix in the period). The series $\{\phi^J\}$ constitute an orthogonal basis on which ζ can be decomposed. With this aim in view, note that from the divergence theorem, the periodicity condition and the zero motion condition on Γ we have:

$$\int_{S_m}\Delta_y(\phi^J)\zeta\,\mathrm{d}s=\int_{S_m}\Delta_y(\zeta)\phi^J\,\mathrm{d}s$$

This equality, re-expressed with the balance equation of both fields ζ and ϕ^J, reads (no summation on J on the left hand side)

$$\lambda_J\int_{S_m}\phi^J\zeta\,\mathrm{d}s=\omega^2\rho_m\int_{S_m}(1+\zeta)\phi^J\,\mathrm{d}s$$

Then, the orthogonality of the eigenfunctions enables us to write ζ in the form

$$\zeta=\zeta^1-1=\sum_{J=1}^{\infty}\frac{\int_{S_m}\phi^J ds}{\int_{S_m}(\phi^J)^2 ds}\frac{\phi^J}{\frac{\lambda_J}{\omega^2\rho_m}-1}$$

Therefore, a solution ζ^1 exists when $\omega\neq\omega_J=\sqrt{\frac{\lambda_J}{\rho_m}}$, $J=1,2\ldots$. If $\omega=\omega_J$, the solution exists if $\int_{S_m}\phi^J ds=0$. When this condition is not met, ζ^1 - then the apparent density $\langle\rho^*\rangle$ - is *not bounded* in the vicinity of ω_J and changes its sign if λ_J is a single eigenvalue.

Note also the limit behavior $\zeta^1(\omega,\underline{y})\to 1$ when $\omega\to 0$, indicating that the apparent density tends to the real density at low frequency. Consequently, the feature of $\langle\rho^*\rangle(\omega)$ can be qualitatively summarized as follows:

$$\begin{aligned}&\langle\rho\rangle\leqslant\langle\rho^*\rangle(\omega)\leqslant+\infty \quad \text{for} \quad 0\leqslant\omega\leqslant\omega_1;\\ &-\infty\leqslant\langle\rho^*\rangle(\omega)\leqslant+\infty \quad \text{for} \quad \omega_J\leqslant\omega\leqslant\omega_{J+1}\end{aligned}\tag{23}$$

Furthermore, in the low frequency range, namely $\omega/\omega_1\ll 1$, expanding ζ^1 in the form

$$\zeta^1(\omega,\underline{y})=1+(\omega/\omega_1)^2\eta(\underline{y})+\cdots,$$

we derive that in first approximation $\eta(\underline{y})$ is governed by:

$$\begin{cases}\mu'_m\Delta_y(\eta)=-\rho_m\omega_1^2 & \text{in } S_m\\ \eta=0 & \text{on } \Gamma;\quad \eta\quad S-\text{periodic in } y\end{cases}$$

Multiplying the balance equation by η and integrating on S_m leads, with the usual integral transformations and the boundary conditions, to: $\rho_m\omega_1^2\int_{S_m}\eta dS=\mu'_m\int_{S_m}|\mathrm{grad}_y(\eta)|^2 ds>0$. Thus,

$$\langle\zeta^1\rangle_m=\frac{1}{|S_m|}\int_{S_m}\zeta^1 dS\geqslant 1$$

$$\text{then } \langle\rho^*\rangle\approx\langle\rho\rangle\left(1+a\left(\frac{\omega}{\omega_1}\right)^2\right)$$

$$\text{with}\quad a>0 \text{ when } \omega/\omega_1\ll 1$$

Consequently, the axial dynamics is governed by the following differential equation:

$$cE_p\frac{\partial^2U_1^0}{\partial^2x_1}\approx-\langle\rho\rangle\omega^2\left(1+a\left(\frac{\omega}{\omega_1}\right)^2\right)U_1^0$$

meaning that the Newtonian inertia is corrected by a term proportional to the time second derivative of the acceleration.

The unusual features of $\langle\rho^*\rangle$ are illustrated here below in two particular cases.

4.3.1. Circular inclusion in square period

As an example, let us consider a square period of side l containing a circular inclusion of radius R. Numerical calculations through finite element method have been performed for a surface concentration of inclusion $c=15\%$ (i.e. $R=0.22l$). Functions $\zeta^1(\omega,\underline{y})$ corresponding to different frequencies ($f=0.2f_0$, $f=f_0$, $f=1.4f_0$ and $f=2f_0$, with $f_0=\sqrt{\mu'_m/\rho_m}/l$) are illustrated in Fig. 4. For $f=0.2f_0$, the matrix motion is not uniform, the vibrations are amplified (up to about 18 %) and in phase with the inclusion. This is consistent with the low frequency regime associated with an apparent density higher than the real density. Conversely, for $f=f_0$ motions in phase opposition occur with a magnification of about 1.7. In that case $\int_{S_m}\zeta^1\,\mathrm{d}s<0$. When the frequency increases, the spatial oscillations of motion in the matrix become richer (see cases $f=1.4f_0$ and $f=2f_0$) and the mean value decreases (except at eigen frequencies).

4.3.2. Approximated apparent density: circular inclusion in circular section

An exact knowledge of $\zeta^1(\omega,\underline{y})$, and then of $\langle\rho^*\rangle$, requires the precise description of the period geometry. Con-

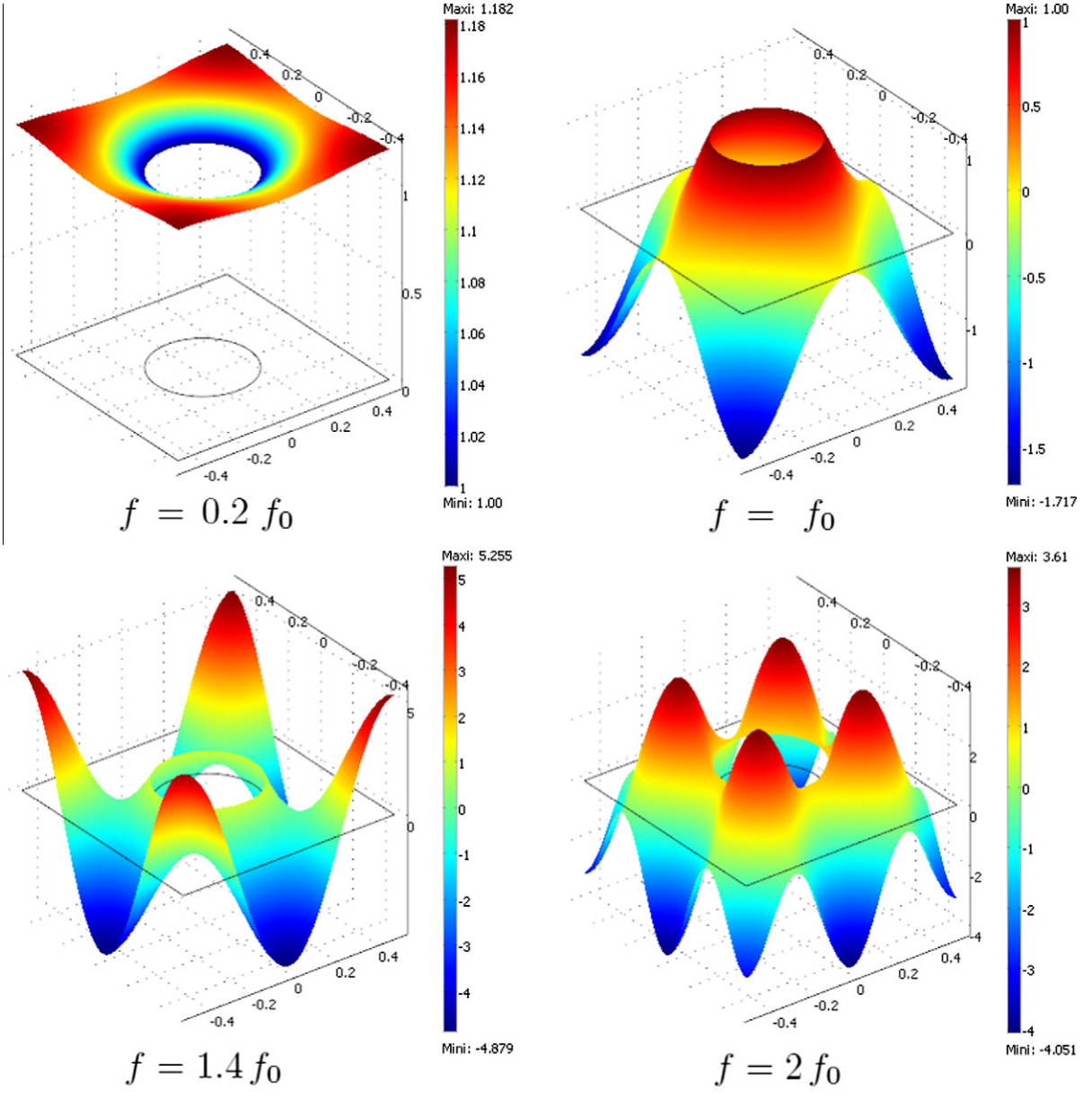

Fig. 4. Finite elements bi-dimensionnal solutions $\zeta^1(\omega, \underline{y})$ of a square period section containing a centered circular inclusion ($c = 15\%$) for different frequency values.

sequently, no general expression can be proposed even for simple geometry (e.g. square or hexagonal symmetry). However, by replacing such a period geometry by a simpler idealized geometry, it becomes possible to determine, a field governed by the same physics as expressed in (19). One may expect that the approximated solution presents similar features to the exact solution. It could also be of interest for practical purposes, e.g. identifying trends as the influence of the inclusion concentration.

The idealized geometry for square or hexagonal periods of section S containing a centered inclusion of section S_p (e.g. circular, hexagonal or square), is a *circular* section (of external radius R_m) of area equal to the period one containing a*centered circular* inclusion (of radius R_p) of area equal to the inclusion one. This implies the following relations:

$$R_m = \sqrt{S/\pi}; \quad R_p = \sqrt{S_p/\pi} = \sqrt{c}R_m; \quad c = \frac{|S_p|}{|S|}$$

With this geometry, it is convenient to use polar coordinates (r, θ) originated at the center of the inclusion. The approximated field ζ^a defined in the matrix domain $(R_p < r < R_m)$ is governed by the same balance equation and Dirichlet boundary condition on $r = R_p$ as ζ^1. However, the periodic boundary condition does not apply to the cir-

cular external periphery $r = R_m$ and other conditions guaranteeing the same physics have to be formulated. In this aim, instead of the periodicity itself, we use the consequence of the periodic assumption in terms of equilibrium and energy. Indeed, the periodic condition imposes that both mean force and mean energy flux on the boundary of the period vanish:

$$\int_{\partial S} \mu'_m \underline{\mathrm{grad}}_y(\zeta^1).\underline{n} ds = 0 \quad \text{and} \quad \int_{\partial S} \mu'_m (\underline{\mathrm{grad}}_y(\zeta^1).\underline{n})\zeta^1 ds = 0$$

By considering the approximated problem, as ζ^a only depends on r (and not on θ) and $\underline{n} = \underline{e}_r$, the gradient normal component reduces to $\underline{\mathrm{grad}}_y(\zeta^1).\underline{n} = \frac{\partial \zeta^a}{\partial r}$. Then both integrals yield:

$$2\pi R_m \mu'_m \frac{\partial \zeta^a}{\partial r}(r = R_m) = 0$$

$$\text{and} \quad 2\pi R_m \mu'_m \frac{\partial \zeta^a}{\partial r}(r = R_m) \times \zeta^a(r = R_m) = 0$$

Consequently, the "ersatz" problem governing ζ^a reads

$$\begin{cases} \Delta_y(\zeta^a) + \frac{\rho_m}{\mu'_m}\omega^2 \zeta^a = \frac{\partial^2 \zeta^a}{\partial r^2} + \frac{1}{r}\frac{\partial \zeta^a}{\partial r} + \frac{\rho_m}{\mu'_m}\omega^2 \zeta^a = 0 \quad \text{for} \quad R_p \leqslant r \leqslant R_m \\ \zeta^a(r = R_p) = 1; \quad \frac{\partial \zeta^a}{\partial r}(r = R_m) = 0 \end{cases}$$

The Helmoltz equation is the canonical form of Bessel differential equations of order zero. Thus, ζ^a is a linear combination of the Bessel functions of the first and second kind J_0 and Y_0. Posing $\alpha = \sqrt{\rho_m/\mu'_m}$, and recalling that $J'_0 = -J_1$ and $Y'_0 = -Y_1$, gives:

$$\zeta^a(\omega, r) = \frac{J_0(\alpha\omega r) - A Y_0(\alpha\omega r)}{J_0(\alpha\omega R_p) - A Y_0(\alpha\omega R_p)}$$

$$\text{with} \quad A(\omega, R_m) = \frac{J_1(\alpha\omega R_m)}{Y_1(\alpha\omega R_m)}$$

The mean value of ζ^a is derived by integrating the Helmoltz equation and by using the boundary conditions:

$$\frac{\rho_m}{\mu'_m}\omega^2 \int_{S_m} \zeta^a ds = -\int_{S_m} \Delta_y(\zeta^a) ds = -\int_{\partial S_m} \underline{\mathrm{grad}}_y(\zeta^a).\underline{n} d_{\partial S_m}$$
$$= 2\pi R_p \frac{\partial \zeta^a}{\partial r}(r = R_p)$$

Thus, the dimensionless apparent density of the matrix in the idealized geometry reads (with $\omega* = \alpha\omega R_m$):

$$\langle \zeta^a \rangle_m = \frac{1}{|S_m|}\int_{S_m} \zeta^a ds$$
$$= \frac{2\sqrt{c}}{(1-c)}\frac{1}{\omega*}\frac{J_1(\omega*)Y_1(\sqrt{c}\omega*) - J_1(\sqrt{c}\omega*)Y_1(\omega*)}{J_0(\sqrt{c}\omega*)Y_1(\omega*) - J_1(\omega*)Y_0(\sqrt{c}\omega*)}$$

At low frequency, by expanding Bessel functions, it yields

$$\langle \zeta^a \rangle_m \approx 1 + \left(\frac{\ln(c)}{4(c-1)} + \frac{c-3}{8}\right)(\alpha\omega R_m)^2 \text{ when } \omega \to 0$$

which matches the trends established previously for periodic solutions.

The effects of the inner dynamics – in a frequency range involving several modes of the idealized geometry – are depicted in Fig. 5 which displays the dimensionless inertial factor $\langle \zeta^a \rangle_m$ versus the dimensionless frequency $\omega*$ for inclusion concentrations of $c = 15\%$ and $c = 5\%$. Note the sign inversion of $\langle \zeta^a \rangle_m$ in the vicinity of the poles. As explained for periodic solutions, the infinite values are reached at the eigen frequencies (of the idealized system). Around each of them, the mean motion of the matrix – relatively to the beam motion – switches from an in-phase regime (positive apparent density) to an out-of-phase regime (negative apparent density). Hence, the observed monotonic variations of $\langle \zeta^a \rangle_m$ in each frequency band $[\omega_J, \omega_{J+1}]$ are in accordance with the analysis of the periodic case (see (23)):

$$1 \leqslant \langle \zeta^a \rangle_m \leqslant +\infty \quad \text{for} \quad 0 \leqslant \omega \leqslant \omega_1;$$
$$-\infty \leqslant \langle \zeta^a \rangle_m \leqslant +\infty \quad \text{for} \quad \omega_J \leqslant \omega \leqslant \omega_{J+1},$$

5. Modal analysis

This section investigates the consequences of the specific dynamic behavior, which is non-local in space for transverse motions and non-local in time for axial motions. The study is performed by analyzing the modes of a reinforced layer of finite thickness H in the direction of the beams ($0 \leqslant x_1 \leqslant H$), and of infinite or finite lateral extension D. This latter dimension will be assumed sufficiently large compared to the period size ($D \gg l$) to apply the homogenized modelling and to disregard the effect of the boundary layer on the medium border. Furthermore, we assume the matrix/beam period to be bi-symmetric so that

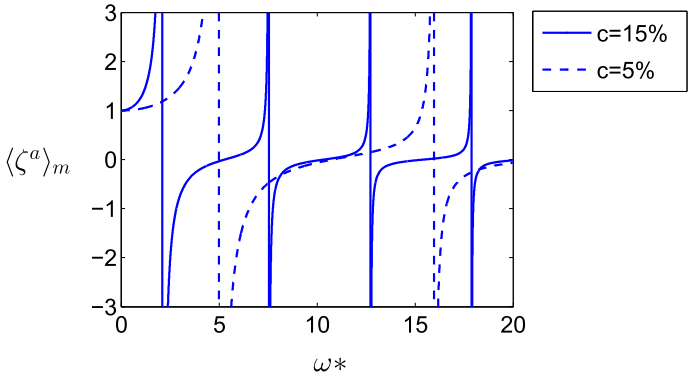

Fig. 5. Dimensionless matrix inertial factor $\langle \zeta^a \rangle_m$ versus the dimensionless frequency $\omega*$ for inclusion concentrations $c = 15\%$ and $c = 5\%$.

the elastic tensor $\underline{\underline{C}}$ is transverse isotropic (hence $C_{11}^{23} = C_{\alpha\alpha}^{23} = C_{1\alpha}^{1\beta} = 0$). $\equiv$

5.1. Transverse modes

As seen in Section 3.4, the kinematics of transverse modes that involves a non-local in space (namely second gradient) effect is either in the form $U_\alpha^0(x_1)\underline{a}_\alpha$ corresponding to a uniform in-plane macroscopic displacement, hence named "homogeneous" modes, or in the form $U_\alpha^0(\underline{x})\underline{a}_\alpha$ corresponding to "inhomogeneous" modes. Both cases are analyzed hereafter.

5.1.1. Boundary conditions

Boundary conditions must be specified at the lower end and at the top of the layer to determine the transverse modal characteristics of the system. Due to the second gradient effect, the conditions involve the motion $U_\alpha^0\underline{a}_\alpha$, the mean stress $\langle\underline{\widetilde{\sigma}}_t^2\rangle$, and also the beam rotation $\partial U_\alpha^0/\partial x_1$ and the beam momentum $E_pI_{p\alpha}\partial^2U_\alpha^0/\partial x_1^2$. Hence, four types of simple boundary conditions are identified:

- Free(F) : $\langle\underline{\widetilde{\sigma}}_t^2\rangle = \underline{0}$ and $E_pI_{p\alpha}\partial^2U_\alpha^0/\partial x_1^2 = 0$
- Clamped(C) : $U_\alpha^0\underline{a}_\alpha = \underline{0}$ and $\partial U_\alpha^0/\partial x_1 = 0$
- Articulated(A) : $U_\alpha^0\underline{a}_\alpha = \underline{0}$ and $E_pI_{p\alpha}\partial^2U_\alpha^0/\partial x_1^2 = 0$
- Sliding(S) : $\langle\underline{\widetilde{\sigma}}_t^2\rangle = \underline{0}$ and $\partial U_\alpha^0/\partial x_1 = 0$

5.1.2. Homogeneous transverse modes

The study of homogeneous transverse modes $U_\alpha^0(x_1)\underline{a}_\alpha$ is based on the following equations obtained from the general model (18):

$$\frac{d}{dx_1}\langle\underline{\widetilde{\sigma}}_t^2\rangle = -\langle\rho\rangle\omega^2U_\alpha^0\underline{a}_\alpha;$$
$$\langle\underline{\widetilde{\sigma}}_t^2\rangle = \left(C_{1\alpha}^{1\beta}\frac{1}{2}\frac{dU_\beta^0}{dx_1} - \frac{E_pI_{p\alpha}}{|S|}\frac{d^3U_\alpha^0}{dx_1^3}\right)\underline{a}_\alpha$$

By considering, for simplicity, motions polarized in the direction $\underline{a}_2$ and by using the following lightened notations $U_2^0 = U$; $x_1 = x$; $I_{p2} = I_p$; $C_{12}^{12} = 2G$, the equilibrium condition verified by the mean displacement U reduces to the scalar equation:

$$-\frac{E_pI_p}{|S|}\frac{d^4U}{dx^4} + G\frac{d^2U}{dx^2} + \langle\rho\rangle\omega^2U = 0 \tag{24}$$

The general solution of this fourth order differential equation (of the same nature as the governing equation of sandwich beams) is in the form:

$$U(x) = a\,\mathrm{ch}\left(\delta_2\frac{x}{H}\right) + b\,\mathrm{sh}\left(\delta_2\frac{x}{H}\right) + c\cos\left(\delta_1\frac{x}{H}\right) + d\sin\left(\delta_1\frac{x}{H}\right)$$
$$\text{with}\quad \begin{cases}\delta_1^2\delta_2^2 = \frac{\omega^2|S|\langle\rho\rangle H^4}{E_pI_p}\\ \delta_2^2 - \delta_1^2 = \frac{G|S|H^2}{E_pI_p} = K\end{cases} \tag{25}$$

where the dimensionless parameter $K = (G|S|H^2)/(E_pI_p)$ "weighs" the bending effects compared to shear effects. Bending predominates when K is small, shear when K is large.

The modal analysis is performed for four pairs of boundary conditions (the first and second conditions correspond respectively to the bottom ($x = 0$) and top ($x = H$)) : clamped-free (CF), clamped-sliding (CS), articulated-sliding (AS) and articulated-free (AF). Each of these conditions is expressed in terms of displacements ($'$ stands for derivative):

- Free condition imposes: $GU' - E_pI_p/|S|U''' = 0$ and $U'' = 0$,
- Clamped condition: $U = 0$ and $U' = 0$,
- Articulated condition: $U = 0$ and $U'' = 0$,
- Sliding condition: $GU' - E_pI_p/|S|U''' = 0$ and $U' = 0$.

Thus, the top and bottom conditions lead to a set of four linear equations. The modes correspond to the non trivial solutions which are obtained when the determinant vanishes. The null-determinant condition results in the modal equations given hereafter for each case:

- Clamped-Free: $\frac{K}{\delta_1^2\delta_2^2} + \frac{\mathrm{th}(\delta_2)\tan(\delta_1)}{\delta_1\delta_2} + \frac{2}{K}\left(1 + \frac{1}{\cos(\delta_1)\mathrm{ch}(\delta_2)}\right) = 0$
- Clamped-Sliding: $\tan(\delta_1) + \frac{(\delta_1^2+K)}{\delta_1\delta_2}\mathrm{th}(\delta_2) = 0$
- Articulated-Sliding: $\cos(\delta_1) = 0$
- Articulated-Free: $(K + \delta_1^2)\mathrm{th}(\delta_2) - \frac{\delta_1^3}{\delta_2}\tan(\delta_1) = 0$

For each case, the modal equation can be solved numerically as a function of K to derive the solutions δ_{1i} and δ_{2i} corresponding to the ith mode. Eigen frequencies and mode shapes of the reinforced layer can then be derived. As an example, Figs. 6 and 7 respectively depict the variation, according to K, of eigen frequencies ratios $f_i/f_1 = (\delta_{1i}\delta_{2i})/(\delta_{11}\delta_{21})$ and of mode shapes for the first three modes under the clamped-free boundary conditions. As expected, it appears in Fig. 6 that for small values of K (dominating bending) the reinforced medium has the same frequency distribution as a clamped-free bending beam (namely $f_i/f_1 = 1; 6.27; 17.55; \ldots$), and for large values of K (dominating shear) f_i/f_1 ratios are close to those of a clamped-free shear layer (i.e. $1; 3; 5; \ldots$). Logically, mode shapes depicted in Fig. 7 vary from bending to shear mode shapes as K increases. Similar trends are observed with the others boundary conditions.

5.1.3. Inhomogeneous transverse modes

To study inhomogeneous transverse modes (of motion polarized for example in the direction $\underline{a}_2$) we introduce in the homogenized model (18) a transverse motion field at the leading order of the form $U_2^0(\underline{x})\underline{a}_2$. By accounting for the transverse isotropy of the elastic tensor, the *in-plane* macro-equilibrium at the leading order gives the set:

$$-\frac{E_pI_p}{|S|}\frac{\partial^4U_2^0}{\partial x_1^4} + \frac{C_{12}^{12}}{2}\frac{\partial^2U_2^0}{\partial x_1^2} + C_{22}^{22}\frac{\partial^2U_2^0}{\partial x_2^2} + \frac{C_{23}^{23}}{2}\frac{\partial^2U_2^0}{\partial x_3^2} + \langle\rho\rangle\omega^2U_2^0 = 0 \tag{26}$$
$$\left(C_{33}^{22} + \frac{C_{23}^{23}}{2}\right)\frac{\partial^2U_2^0}{\partial x_2\partial x_3} = 0 \tag{27}$$

Equation (27) imposes an affine dependance according either to x_2 or to x_3, and the general solution is split in two fields (a_α and b_α are constant coefficients):

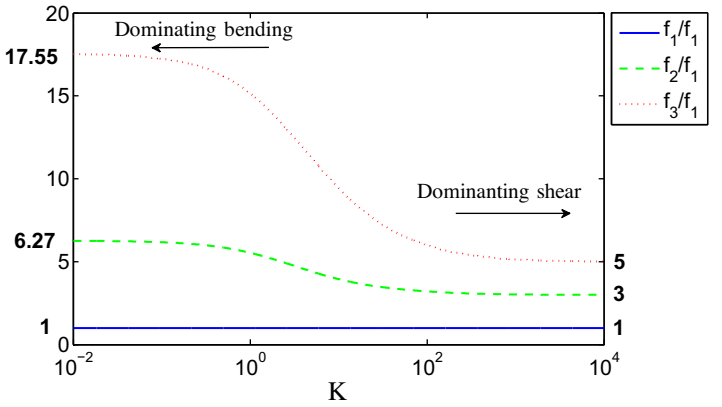

Fig. 6. Variation of the eigen frequencies ratios versus K for clamped-free boundary conditions.

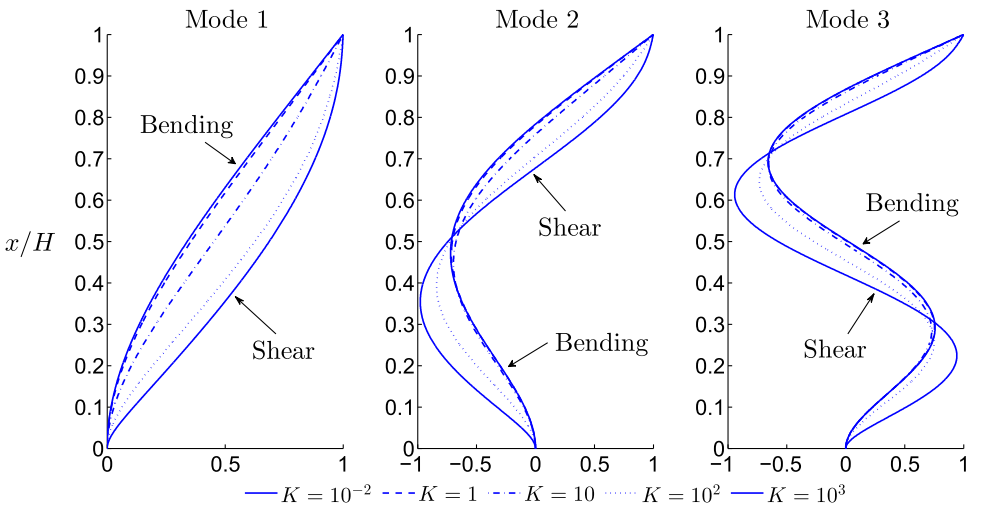

Fig. 7. Mode shapes evolution versus K for clamped-free boundary conditions.

$\underline{U}^0 = (A(x_1,x_2)(a_3x_3+b_3)+B(x_1,x_3)(a_2x_2+b_2))\underline{a}_2$

Both kind of fields (related to A and B) can be studied independently, and in each case the linear dependence simplifies. It leads to focusing on generic solutions in the form (disregarding the linear dependence on the "third" variable):

$\underline{U}^0 = U_2^0(x_1,x_2)\underline{a}_2$ or $\underline{U}^0 = U_2^0(x_1,x_3)\underline{a}_2$

Fields $U_2^0(x_1,x_2)$ are investigated as variables separated functions, i.e. $U_2^0(x_1,x_2) = h(x_1)\times g(x_2)$. Introducing this expression in (26) and dividing by $h(x_1)\times g(x_2)$, leads to the two following equations governing $h(x_1)$ and $g(x_2)$:

$$-\frac{E_pI_p}{|S|}h'''' + \frac{C_{12}^{12}}{2}h' + \langle\rho\rangle\omega^2(1-\beta)h = 0$$
$$\text{and}\quad C_{22}^{22}g'' + \langle\rho\rangle\omega^2\beta g = 0 \qquad (28)$$

where β is a constant to be determined according to the boundary conditions. Note that fields $U_2^0(x_1,x_3) = h(x_1)\times g(x_3)$ lead to same equations (28) except that C_{22}^{22} is replaced by $C_{23}^{23}/2$.

As an example, consider a slot of reinforced medium of height H, of infinite lateral extension along x_3 (hence there is no x_3 dependence in the modes) and of finite lateral extension D along x_2 ($-D/2 \leqslant x_2 \leqslant D/2$). By assuming that the lateral surfaces $x_2 = \pm D/2$ are free of stress, we have:

$$\widetilde{\sigma}_{22}(x_1,\pm D/2) = C_{22}^{22}\frac{\partial U_2^0}{\partial x_2}(x1,\pm D/2) = 0$$
$$\text{therefore}\quad \frac{dg}{dx_2}(\pm D/2) = 0$$

For $\beta < 0$, g takes the form $g(x_2) = a\text{ch}(\delta x_2) + b\text{sh}(\delta x_2)$, with $\delta = \sqrt{\langle\rho\rangle\omega^2|\beta|/C_{22}^{22}}$, and the boundary conditions on lateral faces cannot be satisfied. Thus β must be positive, and g is in the form $g(x_2) = a\cos(\delta x_2) + b\sin(\delta x_2)$. Consequently, the boundary conditions can be fulfilled provided that β takes positive discrete values β_n, each of these values associated with a function $g_n(x_2)$ characterizing compression modes in the direction $\underline{a}_2$:

$$\langle\rho\rangle\omega^2\beta_n = C_{22}^{22}\left(\frac{n\pi}{D}\right)^2 \quad n \in \mathbb{N}$$

and $\quad g_n(x_2) = a_n \cos\left(\frac{2n\pi x_2}{D}\right) + b_n \sin\left(\frac{(2n+1)\pi x_2}{D}\right)$

Equation (28) which governs h and equation (24) which defines homogeneous modes simply differ by the inertial coefficient $(1-\beta_n)$ which may either be positive (e. g. homogeneous modes reached when $n=0$, i.e. $\beta_n = 0$) or negative (e.g. for large transverse compression modes orders n). By introducing the index n to specify the solution, the roots of the characteristic equation of the h_n function (associated with β_n) deduced from (28) read:

$$\begin{cases} \delta_{1n}^2\delta_{2n}^2 & = \frac{\omega^2\langle\rho\rangle(1-\beta_n)|S|H^4}{E_pI_p} = \frac{|S|H^4}{E_pI_p}\left(\omega^2\langle\rho\rangle - C_{22}^{22}\left(\frac{n\pi}{D}\right)^2\right) \\ \delta_{2n}^2 - \delta_{1n}^2 & = \frac{C_{12}^{12}|S|H^2}{2E_pI_p} = K \end{cases}$$

Thus, if $1-\beta_n > 0$, then $\delta_{1n}^2\delta_{2n}^2 > 0$ and we have, similarly to homogeneous modes (25), an oscillating solution of the form:

$$h_n(x_1) = a\mathrm{ch}\left(\delta_{2n}\frac{x_1}{H}\right) + b\mathrm{sh}\left(\delta_{2n}\frac{x_1}{H}\right) + c\cos\left(\delta_{1n}\frac{x_1}{H}\right) + d\sin\left(\delta_{1n}\frac{x_1}{H}\right)$$

Whereas, if $1-\beta_n < 0$, then $\delta_{1n}^2\delta_{2n}^2 < 0$ and we obtain a combination of exponential solutions that correspond to modes confined in the vicinity of the top and bottom boundaries:

$$h_n(x_1) = a\mathrm{ch}\left(\delta_{2n}\frac{x_1}{H}\right) + b\mathrm{sh}\left(\delta_{2n}\frac{x_1}{H}\right) + c\mathrm{ch}\left(\delta_{1n}\frac{x_1}{H}\right) + d\mathrm{sh}\left(\delta_{1n}\frac{x_1}{H}\right)$$

Nevertheless, in both cases, top and bottom boundary conditions expressed through $U(x)$ for homogeneous modes can be directly transposed to $h_n(x_1)$. Therefore, modal equations of inhomogeneous modes are identical to those of homogeneous modes derived in paragraph 5.1.2 except that δ_1 and δ_2 have to be replaced by δ_{1n} and δ_{2n} for $0 < \beta_n < 1$ or by $i\delta_{1n}$ (with $i^2 = -1$) and δ_{2n} for $\beta_n > 1$. The modal frequencies $f_{n/j}$ are now characterized by the order n of the compression modes (along x_2) and the order j of the associated transverse modes (along x_1):

$$f_{n/j} = \frac{1}{2\pi H^2}\sqrt{\frac{E_pI_p}{\langle\rho\rangle|S|}}\sqrt{\delta_{1n/j}^2\delta_{2n/j}^2 + \left(\frac{n\pi}{D}\right)^2\frac{C_{22}^{22}|S|H^4}{E_pI_p}}$$

and the corresponding mode shapes read:

$${}^{inhom}\Phi_{n/j}^0(x_1,x_2) = h_{n/j}(x_1)\times g_n(x_2)$$

In Fig. 8, an illustration of mode shapes ${}^{inhom}\Phi_{n/1}^0(x_1,x_2)$ coupling the first transverse mode ($j=1$) for each of the first three lateral compression modes (n = 1, 2, 3), is presented for a reinforced medium of parameter $K=10$ with clamped-free boundary conditions.

Remark: As mentioned in Section 3.4, an axial corrector $\widetilde{U}_1^2$ arises from the axial balance. In the present case ($U_2^0(x_1,x_2)$), this latter simplifies into:

$$-E_p\frac{|S_p|}{|S|}\frac{\partial^2\widetilde{U}_1^2}{\partial x_1^2} = \left(C_{11}^{22} + \frac{C_{12}^{12}}{2}\right)\frac{\partial^2 U_2^0}{\partial x_1\partial x_2} = \left(C_{11}^{22} + \frac{C_{12}^{12}}{2}\right)h'(x_1)g'(x_2)$$

which enables, with the *axial* boundary condition, the determination of $\widetilde{U}_1^2$.

5.2. Axial modes

As seen in Section 4.2, the kinematics of axial modes that involves non-local in time effect is in the form $U_1^0(\underline{x})\underline{a}_1$.

Here again, boundary conditions must be specified at the lower end and at the top of the layer to determine the axial modal characteristics of the system. At the lead-

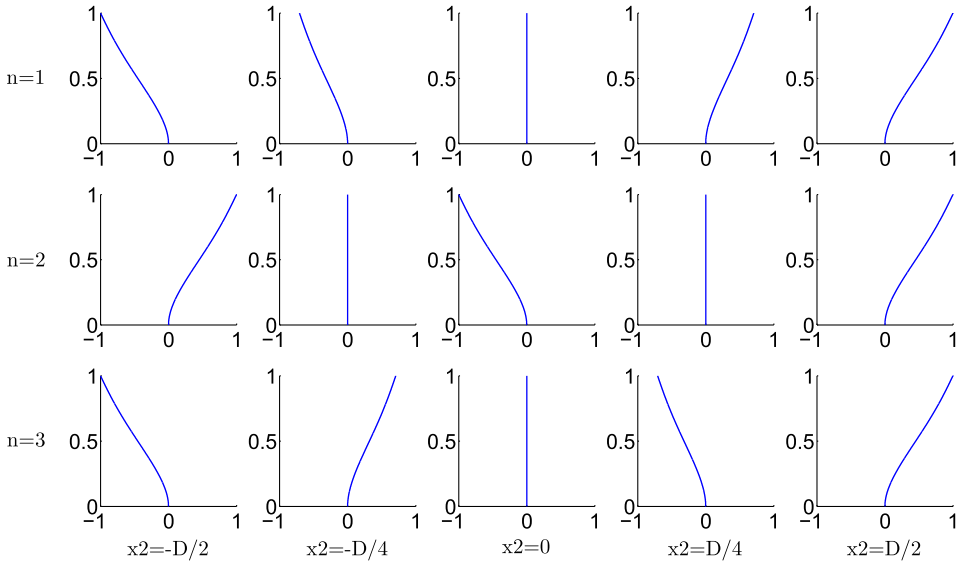

Fig. 8. Inhomogeneous mode shapes ($j=1$, $n=1;2;3$) of a reinforced medium of parameter $K=10$ with clamped-free boundary conditions.

ing order, only the scalar normal stress and strain are involved. Consequently, only two types of boundary conditions apply (note that for the axial kinematics, bending disappears, thus clamped and sliding conditions are respectively equivalent to articulated and free conditions):

$$-\ \text{Free(F)} : \langle \sigma_{\text{n}}^0 \rangle = 0$$
$$-\ \text{Clamped(C)} : U_1^0 = 0$$

The scalar nature of these conditions departs from the usual vectorial conditions. This specificity results from high contrast and high anisotropy; however, it does not induce any indetermination. Indeed, the complementary vectorial conditions arise at the second order and read (accounting for the leading order kinematics):

$$-\ \text{Free(F)} : \langle \tilde{\sigma}_{\text{n}}^2 \rangle \underline{a}_1 + \langle \underline{\tilde{\sigma}}_{\text{t}}^2 \rangle = \underline{0};\quad \langle \underline{\tilde{\sigma}}_{\text{t}}^2 \rangle = \left(\frac{C_{1\alpha}^{1\alpha}}{2} \frac{\partial U_1^0}{\partial x_\alpha} - E_p \frac{I_{p\alpha}}{|S|} \frac{\partial^3 U_1^0}{\partial x_1^2 \partial x_\alpha} \right) \underline{a}_\alpha$$
$$-\ \text{Clamped(C)} : \underline{\tilde{U}}^2 = \underline{0} \tag{29}$$

By associating the axial macroscopic equilibrium and constitutive law (22) derived in paragraph 4.2 in the frequency range $\omega = O(\omega_p)$, the second order differential equation verified by U_1^0 reads:

$$c E_p \frac{\partial^2 U_1^0}{\partial x_1^2} + \langle \rho * \rangle(\omega) \omega^2 U_1^0 = 0 \tag{30}$$

This equation is formally identical to the classic compression dynamic equilibrium, while the apparent density varies with the frequency. The general solution takes the form:

$$U_1^0(x_1, x_2, x_3) = a(x_2, x_3) \cos\left(\delta \frac{x_1}{H}\right) + b(x_2, x_3) \sin\left(\delta \frac{x_1}{H}\right)$$
$$\text{with} \quad \delta = \omega H \sqrt{\frac{\langle \rho * \rangle(\omega)}{c E_p}} \tag{31}$$

To go further in the determination of U_1^0, we have to specify the boundary conditions. Consider for instance a reinforced layer clamped at the bottom and free at the top. Then:

$$U_1^0(0, x_2, x_3) = 0, \quad c E_p \frac{\partial U_1^0}{\partial x_1}(H, x_2, x_3) = 0$$

and therefore: $U_1^0(x_1, x_2, x_3) = b(x_2, x_3) \sin\left(\delta_n \frac{x_1}{H}\right)$ with $\delta_n = \frac{\pi}{2}(2n-1)$. Expressing now the free boundary condition on the top at the second order (29), gives for both tangential stress:

$$\frac{\partial b(x_2, x_3)}{\partial x_\alpha} \left(\frac{C_{1\alpha}^{1\alpha}}{2} + \delta_n^2 E_p \frac{I_{p\alpha}}{|S| H^2} \right) = 0 \text{ then } b(x_2, x_3) = b$$

Consequently, $U_1^0 = b \sin\left(\delta_n \frac{x_1}{H}\right)$, and the mode shapes are identical to those prevailing in classic media in absence of inner resonance. Thus, the orthogonality of eigen modes remains valid. However, both situations differ drastically because of the frequency dependence of $\langle \rho * \rangle$ as described in (23). The essential differences with the usual modal analysis concern the relation between eigen modes and eigen frequencies at the macroscopic scale, as underlined below:

- as $\langle \rho^* \rangle(\omega)$ continuously varies between $\langle \rho \rangle$ and $+\infty$ for $\omega < \omega_1$, all mode shapes at the global scale ($1 \leqslant n < +\infty$) are reached in the *finite* frequency band $[0, \omega_1]$ (ω_1 being the first inner eigen mode of the matrix in the period),
- since $\langle \rho^* \rangle(\omega)$ varies between $-\infty$ and $+\infty$ for $\omega_J \leqslant \omega \leqslant \omega_{J+1}$, the same phenomenon occurs in each frequency band $[\omega_J, \omega_{J+1}]$ defined by the series of eigen frequencies of the periodic inner modes,
- as a consequence, the *n*th mode shape at the global scale is reached for an infinite discrete spectrum frequency ω_{nJ}, each value ω_{nJ} lying between the *J*th and the (*J*+1)th eigen frequencies of the periodic inner modes,
- moreover, since $\langle \rho * \rangle \to +\infty$, when $\omega \to \omega_J$, in the vicinity of each inner eigen frequency, an infinite number of mode shapes is possible. This implies a *concentration* of macroscopic modes in an infinite series of narrow bands around each ω_J of the periodic inner modes.
- finally, recall that δ_n are real whatever the thickness H of the layer. Consequently, the medium presents band gaps in the sense that, independently of H, the eigen frequency of the layer necessarily excludes the frequencies belonging to the series of frequency bands in which $\langle \rho * \rangle < 0$.

Note, however, that these theoretical conclusions must be tempered in practice. First, because real cases necessarily involve damping, implying that $\langle \rho^* \rangle(\omega)$ does not reach infinite values. Second, because the description becomes irrelevant when the scale separation is absent.

6. Conclusion

The effective dynamic behavior of elastic materials periodically reinforced by linear slender elastic inclusions of high stiffness has been derived through the asymptotic homogenization method of periodic media considering different frequency ranges. The behavior of such media with a stiffness contrast of order two significantly departs from the behavior of usual composites.

Two distinct non-local effects, both significant at the leading order, are present concurrently: spatial non-locality traduced by a generalized inner bending behavior, and time non-locality corresponding to a metamaterial behavior. The high stiffness contrast associated with the oriented fiber geometry also implies a high level of anisotropy. Consequently, the motions are strongly oriented according to the anisotropy directions. This imposes to split the kinematics in "transverse and axial" categories, a specific non-local effect being relevant for each of them. Furthermore, the frequency range associated with dynamics in presence of inner bending (e.g. transverse mode) is one order smaller than that associated with dynamics in presence of inner resonance (axial compression mode). Hence, the order of magnitude of diffraction frequencies depends on the propagation mode.

Axial and transverse (homogeneous and inhomogeneous) modes properties of such system differ signifi-

cantly from those of usual composites. In presence of inner bending, the modes shapes and frequency distributions are modified. Nevertheless, the classic general framework of modal analysis remains valid. In presence of inner resonance, the modes shapes are usual. However, the basic principle of the modal analysis, stating that a mode is associated with a single frequency, is lost.

All the constitutive parameters can either be computed rigorously, or be simply estimated from the self consistent approach, with an excellent approximation for weak concentrations of fibers. Such atypical properties can be of interest, either to improve the understanding of the actual behavior of this kind of media (encountered e.g. at large scale in civil engineering) or to design new types of materials (for instance nanomaterials) with tuned dynamic response. Indeed, recent experiments on foam-matrix/steel-fiber evidence the inner bending effect on the fundamental mode shape in accordance with theoretical results (Soubestre et al., 2011).

The extension of the homogenized model to visco-elastic constituents is straightforward when complex modulus (in the Fourier domain) are introduced. Similarly, the global behavior of elastic fibers embedded in a viscous matrix can also be addressed. The influence of damping, on the inner resonance effect, remains to be studied. The perfect contact condition between constituents could also be modified by introducing elastic or visco-elastic interface laws. Further, note that 3-D cells with *unconnected* fibers (to keep inner bending) oriented in the three orthogonal directions, could be addressed similarly. This morphology would lead to the same type of inner bending and inner resonance generalized media, highly anisotropic by construction, presenting nevertheless identical properties in the three directions.

Appendix A. Appendix

By linearity, the solution ${}^{m}u^{1}$ of the problem (8) is in the form

$${}^{m}u^{1} = \left(\psi^{1\alpha}\left[\underline{\mathrm{e}}_{xt}(\underline{U}^{0})\right]_{\alpha}\right)\underline{a}_{1} + \underline{\psi}^{\alpha\beta}\left[\underline{\underline{\mathrm{e}}}_{xs}(\underline{U}^{0})\right]_{\alpha\beta} + v_p\underline{\psi}^{11}\frac{\partial U_1^0}{\partial x_1} + \underline{U}^{1}$$

where ψ^{ij} functions are solutions of elementary problems with $\left[\underline{\underline{\mathrm{e}}}_{x}(\underline{U}^{0})\right]_{ij} = 1$. Consequently, the stress tensor ${}^{m}\underline{\underline{\sigma}}^{2}$ reads:

$$\begin{bmatrix} {}^{m}\sigma_{11}^{2} \\ {}^{m}\sigma_{22}^{2} \\ {}^{m}\sigma_{33}^{2} \\ {}^{m}\sigma_{23}^{2} \\ {}^{m}\sigma_{13}^{2} \\ {}^{m}\sigma_{12}^{2} \end{bmatrix} = \begin{bmatrix} c'^{11}_{11} & c'^{22}_{11} & c'^{33}_{11} & c'^{23}_{11} & 0 & 0 \\ c'^{11}_{22} & c'^{22}_{22} & c'^{33}_{22} & c'^{23}_{22} & 0 & 0 \\ c'^{11}_{33} & c'^{22}_{33} & c'^{33}_{33} & c'^{23}_{33} & 0 & 0 \\ c'^{11}_{23} & c'^{22}_{23} & c'^{33}_{23} & c'^{23}_{23} & 0 & 0 \\ 0 & 0 & 0 & 0 & c'^{13}_{13} & c'^{12}_{13} \\ 0 & 0 & 0 & 0 & c'^{13}_{12} & c'^{12}_{12} \end{bmatrix} \begin{bmatrix} \mathrm{e}_{x11}(\underline{U}^{0}) \\ \mathrm{e}_{x22}(\underline{U}^{0}) \\ \mathrm{e}_{x33}(\underline{U}^{0}) \\ \mathrm{e}_{x23}(\underline{U}^{0}) \\ \mathrm{e}_{x13}(\underline{U}^{0}) \\ \mathrm{e}_{x12}(\underline{U}^{0}) \end{bmatrix}$$

where (without summation on repeated indices)

$$c'^{11}_{11} = \lambda'_m(1 + v_p\mathrm{div}_y(\underline{\psi}^{11})) + 2\mu'_m;$$

$$c'^{11}_{23} = 2\mu'_m v_p \mathrm{e}_{y23}(\underline{\psi}^{11})$$

$$c'^{\alpha\alpha}_{11} = \lambda'_m(1 + \mathrm{div}_y(\underline{\psi}^{\alpha\alpha}));$$

$$c'^{\alpha\alpha}_{23} = 2\mu'_m \mathrm{e}_{y23}(\underline{\psi}^{\alpha\alpha})$$

$$c'^{23}_{11} = 2\lambda'_m \mathrm{div}_y(\underline{\psi}^{23});$$

$$c'^{23}_{23} = 2\mu'_m(1 + 2\mathrm{e}_{y23}(\underline{\psi}^{23}))$$

$$c'^{11}_{\alpha\alpha} = \lambda'_m(1 + v_p\mathrm{div}_y(\underline{\psi}^{11})) + 2\mu'_m v_p \mathrm{e}_{y\alpha\alpha}(\underline{\psi}^{11});$$

$$c'^{1\alpha}_{1\alpha} = 2\mu'_m(1 + 1/2\partial\psi^{1\alpha}/\partial y_\alpha)$$

$$c'^{\beta\beta}_{\alpha\alpha} = \lambda'_m(1 + \mathrm{div}_y(\underline{\psi}^{\beta\beta})) + 2\mu'_m(\delta_{\alpha\beta} + \mathrm{e}_{y\alpha\alpha}(\underline{\psi}^{\beta\beta}));$$

$$c'^{12}_{13} = \mu'_m \partial\psi^{12}/\partial y_3$$

$$c'^{23}_{\alpha\alpha} = 2(\lambda'_m \mathrm{div}_y(\underline{\psi}^{23}) + 2\mu'_m \mathrm{e}_{y\alpha\alpha}(\underline{\psi}^{23}));$$

$$c'^{13}_{12} = \mu'_m \partial\psi^{13}/\partial y_2$$

The expressions of the fields ${}^{p}\underline{u}^{2}$, ${}^{p}\underline{\underline{\mathrm{e}}}^{1}$ and ${}^{p}\underline{\underline{\sigma}}^{1}$ solutions of the Neumann problem (9) are detailed hereafter:

$$\begin{aligned} {}^{p}\underline{u}^{2} = \Bigg(& \frac{\partial^2 U_1^0}{\partial x_1^2} v_p \frac{\left\|\underline{y}\right\|^2}{2} + \underline{y}.\underline{\mathrm{grad}}_x(\underline{\mathrm{e}}_{xt}(\underline{U}^{0}).\underline{y}) + \frac{1}{2}\underline{y}.\left[\underline{\underline{\mathrm{e}}}_{xs}(\underline{U}^{0})\right]_{,x_1}.\underline{y} \\ & + \frac{1}{2}\left(\frac{\partial^2 U_3^0}{\partial x_1 \partial x_2} - \frac{\partial^2 U_2^0}{\partial x_1 \partial x_3}\right) W + \frac{\partial^p \Theta^0}{\partial x_1} W - 2\underline{y}.\underline{\mathrm{e}}_{xt}(U_1^1\underline{a}_1 \\ & + U_\alpha^1\underline{a}_\alpha))\underline{a}_1 - v_p\frac{\partial U_1^1}{\partial x_1}\underline{y} - \underline{\underline{\mathrm{e}}}_{xs}(U_\alpha^1\underline{a}_\alpha).\underline{y} \\ & + \frac{1}{2}v_p\left\|\underline{y}\right\|^2 \underline{\mathrm{grad}}_{xs}\left(\frac{\partial U_1^0}{\partial x_1}\right) + 2v_p([\underline{\mathrm{e}}_{xt}(\underline{U}^{0})]_{\alpha})_{,x_1}\underline{\xi}^{\alpha} \\ & + \frac{1}{2}\underline{\mathrm{grad}}_{xs}(\underline{y}.\underline{\underline{\mathrm{e}}}_{xs}(\underline{U}^{0}).\underline{y}) - \frac{\partial^p \Theta^0}{\partial x_\alpha}\underline{a}_1 \wedge y_\alpha\underline{y} + {}^{p}\Theta^{1}\underline{a}_1 \wedge \underline{y} \\ & + {}^{p}\underline{U}^{2} \end{aligned}$$

$${}^{p}\underline{\underline{\mathrm{e}}}^{1} = \frac{\partial^p u_1^1}{\partial x_1}\left[\underline{a}_1 \otimes \underline{a}_1 - v_p\underline{\underline{I}}_s\right] + ({}^{p}\underline{\mathrm{e}}_{\mathrm{t}}^{1} \otimes \underline{a}_1 + \underline{a}_1 \otimes {}^{p}\underline{\mathrm{e}}_{\mathrm{t}}^{1})$$

$${}^{p}\underline{\underline{\sigma}}^{1} = E_p\frac{\partial^p u_1^1}{\partial x_1}[\underline{a}_1 \otimes \underline{a}_1] + ({}^{p}\underline{\sigma}_{\mathrm{t}}^{1} \otimes \underline{a}_1 + \underline{a}_1 \otimes {}^{p}\underline{\sigma}_{\mathrm{t}}^{1})$$

$$\begin{aligned} \text{with} \quad {}^{p}\underline{\mathrm{e}}_{\mathrm{t}}^{1} = & \left(\frac{1}{2}\left(\frac{\partial^2 U_3^0}{\partial x_1 \partial x_2} - \frac{\partial^2 U_2^0}{\partial x_1 \partial x_3}\right) + \frac{\partial^p \Theta^0}{\partial x_1}\right)\frac{1}{2}(\underline{\mathrm{grad}}_y(W) \\ & + \underline{a}_1 \wedge \underline{y}) \end{aligned}$$

$$\begin{aligned} {}^{p}\underline{\sigma}_{\mathrm{t}}^{1} = & \left(\frac{1}{2}\left(\frac{\partial^2 U_3^0}{\partial x_1 \partial x_2} - \frac{\partial^2 U_2^0}{\partial x_1 \partial x_3}\right) + \frac{\partial^p \Theta^0}{\partial x_1}\right)\mu_p(\underline{\mathrm{grad}}_y(W) + \underline{a}_1 \\ & \wedge \underline{y}) \end{aligned}$$

where $\underline{\xi}^{\alpha} = y_\alpha\underline{y} - \frac{1}{2}\left\|\underline{y}\right\|^2\underline{a}_\alpha$ and $W(y_2, y_3)$, the wrapping function of the beam section, verifies the following limit problem defined on S_p:

$$\begin{cases} \Delta_y(W) = 0 & \text{in } S_p \\ \underline{\text{grad}}_y(W).\underline{n} = -(\underline{a}_1 \wedge \underline{y}).\underline{n} & \text{on } \Gamma \\ \int_{S_p} W ds = 0 & (\text{uniqueness}) \end{cases}$$

The macroscopic elastic tensor $\underline{\underline{\underline{\underline{C}}}}$ and the scalar $\mathcal{J}_{p\alpha}$ involved in the macroscopic description (14) have the following expressions:

$$C^{ij}_{11} = \varepsilon^2 C'^{ij}_{11}; \quad C^{ij}_{\alpha\beta} = \varepsilon^2 C'^{ij}_{\alpha\beta}; \quad C^{1\beta}_{1\alpha} = \varepsilon^2 C'^{1\beta}_{1\alpha};$$

$$\mathcal{J}_{p\alpha} = \varepsilon^4 \mathcal{J}'_{p\alpha} \quad \text{with} \quad \{ij\} = \{11, 22, 33, 23\}$$

$$\text{where } C'^{ij}_{11} = \frac{1}{|S'|}\left(\int_{S_m} c'^{ij}_{11} ds + v_p \int_{\Gamma} y_\alpha c'^{ij}_{\alpha\delta} n_\delta d\gamma\right)$$

$$C^{ij}_{\alpha\beta} = \frac{1}{|S'|}\int_{\partial S} y_\alpha c'^{ij}_{\beta\delta} n_\delta d\gamma$$

$$C^{1\beta}_{1\alpha} = \frac{1}{|S'|}\int_{\partial S} y_\alpha c'^{1\beta}_{1\delta} n_\delta d\gamma \quad \mathcal{J}'_{p\alpha} = \left((-1)^\alpha I'_{p\alpha} + \int_{S_p} y_\alpha \frac{\partial W}{\partial y_{\bar{\alpha}}} ds\right)$$

References

Auriault, J.L., 1991. Heterogeneous medium. Is an equivalent description possible? Int. J. Eng. Sci. 29 (7), 785–795.

Auriault, J.L., Bonnet, G., 1985. Dynamique des composites èlastiques périodiques. Arch. Mech. 37 (4–5), 269–284.

Ávila, A., Griso, G., Miara, B., 2005. Bandes phoniques interdites en élasticité linéarisée. C.R. Acad. Sci. Paris, Ser. I 340, 933–938.

Babych, N.O., Kamotski, I.V., Smyshlyaev, V.P., 2008. Homogenization of spectral problems in bounded domains with doubly high contrasts. Networks Heterogen. Media 3 (3), 413–436.

Bellieud, M., Bouchitté, G., 1997. Homogénéisation de problèmes elliptiques en présence de fibres de grande conductivité. C.R. Acad. Sci. Paris, Série I 323, 1135–1140.

Bensoussan, A., Lions, J.L., Papanicolaou, G., 1978. Asymptotic Analysis for Periodic Structures. North-Holland Publishing Company, Amsterdam.

Boutin, C., 1996. Microstructural effects in elastic composites. Int. J. Solids Struct. 33 (7), 1023–1051.

Boutin, C., Auriault, J.L., 1993. Rayleigh scattering in elastic composite materials. Int. J. Eng. Sci. 31 (12), 1669–1689.

Boutin, C., Hans, S., Chesnais, C. 2010. Generalized beam and continua. Dynamics of reticulated structures. in: Maugin, G.A., Metrikine, A.V. (Eds.), Mechanics of generalized continua. Springer, New York, pp. 131–141.

Boutin, C., Soubestre, J., 2011. Generalized inner bending continua for linear fiber reinforced materials. Int. J. Solids Struct. 48, 517–534.

Caillerie, D., 1980. Effect of a thin inclusion of high rigidity in an elastic body. Math. Methods Appl. Sci. 2 (3), 251–270.

Courant, R., Hilbert, D., 1970. Methods of Mathematical Physics I, eighth ed. Interscience Publishers Inc., New York.

De Buhan, P., Sudret, B., 1999. Two-phase elastoplastic model for unidirectionally-reinforced materials. Eur. J. Mech. A/Solids 18 (6), 995–1012.

Dell'Isola, F., Seppecher, P. 1995. The relationship between Edge Contact forces, double forces and interstitial working allowed by the principle of virtual power. Comptes Rendus de L'Academie des Sciences CRAS t. 321, II b, pp. 303–308.

Gambin, B., Kröner, E., 1989. High order terms in homogenized stress–strain relation of periodic elastic media. Phys. Stat. Solids (b) 151, 513–519.

Léné, F., 1978. Comportement macroscopique de matériaux élastiques comportant des inclusions rigides ou des trous répartis périodiquement. C.R. Acad. Sci. Paris, Série IIB 286, 75–78.

Liu, Z., Zhang, X., Mao, Y., Zhu, Y.Y., Yang, Z., Chan, C.T., Sheng, P., 2000. Locally resonant materials. Science 289, 1734–1736.

Pideri, C., Seppecher, P., 1997. Un résultat d'homogénéisation pour un matériau élastique renforcé périodiquement par des fibres élastiques de très grande rigidité. C.R. Acad. Sci. Paris, Série IIb 324 (7), 475–481.

Postel, M. 1985. Réponse sismique de fondations sur pieux. Ph.D thesis, Ecole Centrale de Paris, Paris.

Sanchez-Palencia, E., 1980. Nonhomogeneous media and vibration theory. Lectures Notes in Physics, vol. 127. Springer-Verlag, Berlin.

Smyshlyaev, V.P., 2009. Propagation and localization of elastic waves in highly anisotropic periodic composites via two-scale homogenization. Mech. Mater. 41 (4), 434–447.

Soubestre, J., Boutin, C., Dietz, M.S., Dihoru, L., Hans, S., Ibraim, E., Taylor, C.A., 2011. Dynamic behaviour of reinforced soils – theoretical modelling and shaking table experiments. Geotech. Geolog. Earthquake Eng. 22, 247–263.

Vasseur, J.O., Deymier, P.A., Prantziskonis, G., Hong, G., 1998. Experimental evidence for the existence of absolute acoustic band gaps in two-dimensional periodic composite media. J. Phys. Condens. Mater 10, 6051–6064.

Zhikov, V.V., 2000. On an extension of the method of two-scale convergence and its applications. Sbornick Math. 191 (7–8), 973–1014.